Highlights

- Partially blocked flow channels are proposed for the energy conversion of a PEMFC.
- Effects of geometric parameters on mass transfer and energy performance are observed.
- The enhancement in mass transfer is attributed to the generation of a nozzle-type effect.
- The improvement in both conversion efficiency and effective power is about 17%.

Research Paper

The Mass Transfer Characteristics and Energy Improvement with Various Partially Blocked Flow Channels in a PEM Fuel Cell

Pengcheng Dong [1], Gongnan Xie [1,*], Meng Ni [2]

[1] School of Marine Science and Technology, Northwestern Polytechnical University, Xi'an, 710072, P.R. China.

[2] Building Energy Research Group, Department of Building and Real Estate, The Hong Kong Polytechnic University, Hong Kong, P.R. China.

[*] Corresponding address: School of Marine Science and Technology, Northwestern Polytechnical University, P.O. Box 24, Xi'an, 710072, China. Tel: +86-29-88492611; Fax: +86-29-88495278. E-mail: xgn@nwpu.edu.cn (G. Xie).

Abstract: In order to improve the mass transfer and the energy performance of a Proton Exchange Membrane Fuel Cell (PEMFC), five different kind of block shapes in the flow channel are proposed and evaluated numerically. It is found that the use of blocks in the gas channel enhances the mass transfer due to the generation of a nozzle-type effect in the channel. Results shows that the performances of PEMFCs with the five blocked channels [Cases B-F] can be improved comparing with that of the conventional flow channel without block [Case A], and Case D performs the best. The electrochemical conversion efficiency and effective power are improved by 15.58% and 15.77%, respectively. Further, by observing the block heights (0.4, 0.5 and 0.6) and spatial intervals (2.5, 5.0 and 8.0) of the above optimal shape [Case D] on the energy performances, these improvements can be raised to 17.09% and 16.95%, respectively.

Keywords: PEMFC; Blocked flow channel; Mass transfer; Pressure drop; Effective power; Cell performance.

Nomenclature

a	= water activity / height of block (mm)
b	= parameter of block(mm)
c	= parameter of block(mm) / concentration (mol/m^3)
c_r	= condensation rate constant
F	= Faraday constant (96485 C/mol)
h	= net enthalpy change (J/kg)
H	= Enthalpy (J/kg) / height (mm)/thickness (mm)
i	= transfer current density (A/m^3)
i_0	= reference current density (A/m^2)
M	= molecular weight (kg/mol)
ME	= membrane equivalent weight (kg/mol)

n = direction vector / the number of electron

p = pressure (Pa) / interval of between different block (mm)

r = mass fraction

R = universal gas constant (8.314 J/mol·K) / resistivity ($1/m^2$)

s = water saturation

V = molar volume (m^3/mol) / voltage (V)

W = width (mm)

Y = mass fraction

Greek symbols

α = transfer coefficient

γ = concentration dependence

ε = porosity

ζ = specific active surface area (1/m)

η = local surface over-potential (V) / efficiency

λ = water content

μ = dynamic viscosity (Pa·s)

ξ = stoichiometry ratio

σ = electron / proton conductivity (S/m) / surface tension (N/m^2)

ϕ = potential (V)

Superscripts and Subscripts

a = anode

c = contact / cathode

cc = current collector

cd = computational domain

ch = gas channel

cl = catalyst layer

eff = effective

E = energy equation

gd = gas diffusion layer

i = *i*th species

l = liquid water

L = limited / liquid water

m = membrane

M = mass equation

OUT = output

pascal = loss of energy due to pressure

peak = peak

react = electrochemical reaction

ref = reference

sat = saturation

w = water

wv = water vapor

1. INTRODUCTION

Currently, with the increase of the environmental issue and energy consumption, fossil fuels have failed to meet the demands for an efficient, clean and economical energy system in the future society. Fuel cell is the power generating device that it can directly convert chemical energy into electrical energy. The efficiency of current generation by fuel cell is not limited by the Carnot cycle efficiency [1]. Hydrogen energy possess the property of high efficiency and cleanness, which can make hydrogen an ideal energy carrier. Especially, Proton Exchanger Membrane Exchange Fuel Cell (PEMFC) has become one of the most promising energy storage devices due to its advantages such as low cost, environmental-friendliness and high efficiency and so on. However, further performance improvement and cost reduction are needed for wide application of PEMFC.

As the performance of PEMFC heavily relies on the mass transportation, heat transfer, electrochemical process, electronic and ionic transports processes, extensive research efforts have been made to understand the coupled transport and reaction in the PEMFC. The transport mechanisms about the proton and water molecules in the electrolyte membrane, one key component of the PEMFC, had been investigated [2,3]. The effects of pressure, flow, and temperature on PEMFC's performance and water management were studied to optimize life and durability of PEMFC [4,5]. A two-phase model was developed to simulate the transport of water in gas diffusion layer (GDL) and catalyst layer (CL) considering a micro-porous layer (MPL) [6]. In addition, the energy and exergy efficiency analysis [7] and techno-economic analysis [8] is researched in PEMFC performance improvement and energy production.

Among many factors affecting the PEMFC performance, most important one is the electrochemical reaction, especially, the ORR. On the one hand, the structure and properties of the catalyst itself can greatly affect ORR. Zhao et al. [9] investigated the effect of electrodes on performance based on Pt/C ratio and Pt load. The development of novel catalysts is one of the new ways to improve the performance of PEMFC [10]. On the other hand, the catalyst layer is very difficult to model accurately as it involves multiphysics processes and electrochemical reaction. In the catalyst layer, a two-dimensional agglomerate model was developed by Siegel et al [11]. Sui et al. [12] summarized various models on the transport behaviors in the catalyst layer from macroscopic scale to molecular scale.

In addition to the above factors, the collector plate also greatly affects the performance of PEMFC. An economical and efficient Cr-C coated collector plate is applied to the PEM electrolyzer [13]. Wilberforce et al. [14] found that the performance of coated metal collector plate is better than that of bare metal collector plate. Meanwhile, the flow field of collector plate significantly affect the performance of a practical PEMFC as the flow field distributes gases in the entire PEMFC. The design method of the common existing designs of flow field was comprehensively evaluated and its

disadvantages were improved [15]. The transfer characteristics and performance of PEMFC were investigated based on the Z-type flow-field [16] and the converging-diverging flow field [17]. With the improvement of bionic technology and machining level, some novel flow field structures have been proposed. The characteristics of PEMFC were studied based on flow field using an open pore cellular foam material [18]. Iranzo et al. [19] comprehensively studied the advantages and disadvantages of bionic collector plates based on their biological characteristics. In Ref. [20], The flow field structure mentioned above is fully evaluated and the effect of some parameters (such as flow direction, channel length, using block, etc.) on performance was thoroughly studied, which provided guidance for the efficiency improvement of PEMFC and the optimization of collector plates.

As the smallest basic unit in the flow field--gas flow channels, the wave-like channel has better performance compared with the conventional channel [21]. Yan et al. [22] and Perng et al. [23] studied the structure parameter of installed baffle and acquired the optimal parameters. The optimal design of waveform channel by genetic algorithm is based on bionics principle [24]. However, since the wave-like channels were proposed, various wave-like channels have been studied and evaluated. It is worth noting that although the wave-like channels can improve the overall performance. "What is the optimal structural parameter of the waveform channel?" It has been a hot spot in the direction of PEMFC, so far there is no standard answer. In order to further investigate the effect of different flow channels of block structure on the performance and transmission characteristics of PEMFC, this paper studies the performance improvement from the perspective of curvature. In the conclusion part, the better structural parameters are summarized.

In the paper, a non-isothermal, two-phase flow, laminar, steady state model is developed considering isotropic catalyst layer and anisotropic gas diffusion layer to study the performance of PEMFCs. The three factors: shape, height of the block (a) and interval between different blocks (p) are considered. In the following content, we will analyze and compare the three factors mentioned above. We will analyze the transport behavior and performance fluctuations in the PEMFC with block structures regarding the block curvature from small to large changes in the process. This research work will provide new directions for its further optimization and commercial use in following work.

2. DESCRIPTION OF PHYSICAL MODELS

2.1 Geometrical Models

In the paper, the schematic diagram of a PEMFC with conventional gas flow field is shown in Fig. 1. Fig. 1 (a) can be described as follows: the PEMFC consists of three main parts (i.e., anode, membrane and cathode). The subassemblies of anode and cathode are made of current collector

(CC), gas diffusion layer (GDL) and catalyst layer (CL). The flow direction of electrochemical reaction components and products in the cathode catalyst layer are shown in Fig. 1 (*d*). To simplify our calculation, a computational domain is proposed as shown in Fig. 1 (*e*). The general parameters of the domain are shown in Fig. 1 (*b*) and Fig. 1 (*c*). For the conventional gas flow channel, the ratio of width and height of gas flow channel, W_{ch}/H_{ch} , is equal to 1.0. Some representative surfaces are shown in Fig. 1 (*e*). X1, Y1 and Z1 represent the neutral plane along the *x*-direction(the flow direction), the *y*-direction and the *z*-direction, respectively. Z2 represent the interface between CL and GDL in cathode. Z3 represent the interface between current collector and GDL in cathode. The Line 1 is the intersection of surface Y1 and surface Z2 and Line 2 is the intersection of surface Y1 and surface Z3 is omitted in the Fig. 1 (*e*).

2.2 Computational Domain

Three-dimensional computational domain of PEMFC is shown in Fig. 2 (the current collector is omitted). The research contents in this paper are mainly divided into three categories: the shape of blocks, the height of blocks (*a*), the interval between two neighbouring blocks (*p*). The conventional channel (Case A) is used as the reference baseline in all the cases. The parameters for the computational domain are listed in Table 1. The relationship of other parameters is: $a=2b$, $c=2a$. In all cases, there are five shapes (in terms of section shapes about blocks, semi-circle, thin semi-ellipse, standard semi-ellipse, special-shape profile, half regular hexagon), three heights of blocks (a = 0.4, 0.5, 0.6 mm) and three intervals between the different cases (p = 2.5, 5.0, 8.0 mm), which are designed to investigate their effects on the performance of PEMFC. The detailed information of the cases is listed in Table 2 (Refs [25-30] are applied to Table 2).

3. DETAILS OF NUMERICAL SIMULATIONS

3.1 Assumptions

As a coupling physical field of many physical processes, the mechanism of PEMFC is very complex. In general, we need to make assumptions to simplify the model. The assumptions from the model are as follow:

- All gas component are the in-compressible ideal gases.
- The ideal gas mixing law is applied.
- The flow state is steady and laminar.
- The contact resistances between different layers is neglected.
- The relationship potential and current is satisfied Butler-Volmer equation.
- GDLs are anisotropic and CLs are isotropic.

3.2 Governing Equations

Mass Conservation [31,11]:

$$\nabla \cdot \left(\rho \vec{u} \right) = S_M \tag{1}$$

where ρ is the density of the mixture, S_M is the source term of mass.

Momentum Conservation [33]:

$$\nabla \cdot \left(\rho \vec{u}\vec{u} \right) = -\nabla p + \left(\mu^{eff} \nabla \vec{u} \right) + S_{MOM} \tag{2}$$

where S_{MOM} is the source term of momentum (Darcy's law). p and μ are pressure and dynamic viscosity of the mixture fluid, respectively.

Energy Conservation [32,11]:

$$\nabla \cdot \left(\rho c_p \vec{u} T \right) = \nabla \cdot \left(k_{eff} \nabla T \right) + S_E \tag{3}$$

$$S_E = h_{react} - i_{an,cat} \eta_{an,cat} + I^2 R_{ohm} + h_L \tag{4}$$

where c_p and k_{eff} are the specific heat and effective thermal conductivity, respectively. And S_E is the source term of energy. $\left(h_{react} - i_{an,cat} \eta_{an,cat} \right)$ is the heat generated by the electrochemical reaction, which h_{react} is the net enthalpy difference because of the electrochemical reaction and $i_{an,cat} \eta_{an,cat}$ is the heat generation due to the activation loss of the electrochemical reaction ($i_{an,cat}$ is the exchange current density calculated by the Butler-Volmer equation in the anode or the cathode， $\eta_{an,cat}$ is the over-potential in the anode or the cathode TPB). $I^2 R_{ohm}$ is the joule heating due to the ohmic resistance of transmission media. And the h_L term is the phase-transition enthalpy of water.

Species Conservation [33]:

$$\nabla \cdot \left(\rho \vec{u} Y_i \right) = \nabla \cdot \left(\rho D_i^{eff} \nabla Y_i \right) + S_i \tag{5}$$

here, Y_i, D_i^{eff} and S_i denote the mass fraction of species i, effective diffusivity and the species volumetric source term of the ith species.

Liquid Water transport equation:

The water vapor can condense to liquid water due to low operating temperature. The liquid water may keep the membrane hydrated to ensure the good passage of protons (H^+). It can block the gas diffusion and reduce the active area for reaction. A saturation model has been developed ([34] and [35]) to model the water transport.

$$\nabla \cdot \left[\rho_l \frac{Ks^3}{\mu_l} \frac{dp_c}{ds} \right] = S_w \tag{6}$$

where ρ_l and μ_l are the density and the dynamic viscosity of liquid water, respectively, K is the permeability. The p_c and S_w are the capillary pressure(i.e., the pressure difference between the wetting and non-wetting phase) and the condensation rate, respectively.

$$p_c = \begin{cases} \dfrac{\sigma\cos\theta_c}{(K/\varepsilon)^{0.5}}\left(1.417(1-\mathrm{s}) - 2.12(1-\mathrm{s})^2 + 1.263(1-\mathrm{s})^3\right) & \theta_c < 90° \\ \dfrac{\sigma\cos\theta_c}{(K/\varepsilon)^{0.5}}\left(1.417s - 2.12s^2 + 1.263\mathrm{s}^3\right) & \theta_c > 90° \end{cases} \quad (7)$$

where σ and θ_c are the surface tension and the contact angle, respectively.

$$S_w = c_r \max\left(\left[(1-s)\frac{p_{wv} - p_{sat}}{RT} M_{H_2O}\right], [-s\rho_l]\right) \quad (8)$$

The condensation rate constant is calculated as $c_r = 100s^{-1}$. It is assumed that the liquid water formation rate is equal to the gas velocity of the gas channel. p_{wv} and p_{sat} are the water vapor pressure and the saturation pressure respectively. The water vapor pressure is computed based on Eqs. (9) (i.e., the vapor fraction and the local pressure). The saturation pressure p_{sat} is determined by the temperature.

$$x_{H_2O} = p_{wv} / p \quad (9)$$

Electrochemical Equation [31,32,11]:

The electrochemical reaction takes place in the catalyst layer of the porous electrode, which cause to the release (anode) and "consumption" (cathode) of electrons. The current density, $i_{an,ca}$, being generated in the electrochemical process is displayed by the Butler-Volmer equation in the catalyst of anode and cathode.

$$i_{an} = \left(\zeta_{an} i_{an}^{ref}\right)\left(\frac{C_{H_2}}{C_{H_2}^{ref}}\right)^{\gamma_{an}}\left(e^{\alpha_{an}F\eta_{an}/RT} - e^{-\alpha_{ca}F\eta_{an}/RT}\right) \quad (10)$$

$$i_{ca} = \left(\zeta_{ca} i_{ca}^{ref}\right)\left(\frac{C_{O_2}}{C_{O_2}^{ref}}\right)^{\gamma_{ca}}\left(-e^{\alpha_{an}F\eta_{ca}/RT} + e^{-\alpha_{ca}F\eta_{ca}/RT}\right) \quad (11)$$

where ζ and i^{ref} are the specific active surface area and reference exchange current density per active surface area, respectively. C and C^{ref} denoted the local species concentration and the reference concentration. α is the dimensionless transfer coefficient. η_{an} and η_{ca} are the local surface over-potential (the activation loss) in anode and cathode. The local surface over-potential is the driving power for the kinetics of electrochemistry.

$$\eta_{an} = \phi_s - \phi_m \quad (12)$$

$$\eta_{ca} = \phi_s - \phi_m - V_{OCV} \quad (13)$$

where ϕ_s and ϕ_m are the potential of solid phase and electrolyte phase, respectively. The V_{OCV} term is the open-circuit voltage(the theoretical reversible cell potential).

Charge Conservation [33]:

$$\nabla \cdot \left(\sigma_s^{eff} \nabla \phi_s \right) = -S_s \tag{14}$$

$$\nabla \cdot \left(\sigma_m^{eff} \nabla \phi_m \right) = -S_m \tag{15}$$

where σ_s^{eff} and σ_m^{eff} stand for the effective conductivity of solid phase and electrolyte phase, respectively. The $S_{s,m}$ terms are the volumetric transfer current.

$$S_s = \begin{cases} -i_{an} & \text{(anode)} \\ +i_{ca} & \text{(cathode)} \end{cases} \quad and \quad S_m = \begin{cases} +i_{an} & \text{(anode)} \\ -i_{ca} & \text{(cathode)} \end{cases} \tag{16}$$

Water transport in membrane [36]:

Eq. (16) describes the water transport in the membrane which includes the back diffusion and electro-osmotic effect, given that the convection effect is ignored.

$$\nabla \cdot \left(D_w^{eff} \nabla C_w \right) - \frac{1}{F} \nabla \left(n_d i_e \right) = 0 \tag{17}$$

where D_w^{eff} and C_w are the water diffusivity in membrane and the equivalent water concentration of membrane, respectively. The i_e term is the superficial current density. The osmotic drag coefficient, n_d, is a function of the water content λ. Here, C_w and D_w^{eff} are defined as, respectively.

Based on these governing equations, the source terms of mass, momentum, energy, charge and species are summarized in the **Table 3**.

3.3 Boundary Conditions and Solution Method

In the paper, the boundary conditions were set based on the assumptions and the conservation equations. The flow direction of hydrogen and oxygen is the same at the channels. For the inlet of the channels at anode and cathode, the boundary condition--the mass flow rate $\dot{m} = \int_A \rho \vec{u} \cdot \vec{n} dA$, temperature and species mass fraction--are specified. The water saturation is zero in the inlet of channels. The pressure outlet is applied in the outlet of the channels. Most important, the mass flow rate of hydrogen and oxygen are calculated by the Eqs. (17) and (18). For the terminal of anode and cathode, the temperature is the same as that specified, whereas the potential is zero on anode ($\phi_s = 0$), and is equal to the cells potential on cathode ($\phi_s = V_{cell}$). The key physical parameters and their values applied in the paper are listed in Table 4.

$$\dot{m}_{an,in} \geq \frac{\xi_{H_2}}{r_{H_2}} \frac{M_{H_2}}{2F} i_{an}^{ref} A_m \tag{18}$$

$$\dot{m}_{\mathrm{ca},in} \geq \frac{\xi_{O_2}}{r_{O_2}} \frac{M_{O_2}}{4F} i_{ca}^{ref} A_m \tag{19}$$

The SIMPLE algorithm is applied to combine the continuity equation and the momentum equation deduced the pressure equation. The pressure is adopted to the standard format. For the other items, the first-order upwind schemes are used at the beginning of calculation and the second-order upwind schemes are adopted for accurate calculation.

3.4 Grid Independence and Model Validation

The situation of grid directly affects the accuracy and efficiency of the simulation, the global grid of the computational domain and the local grid near the baffle are shown in Fig. 3 (a) and (b) respectively. The grid independence is examined by Case A (is conventional channels) taken as the reference. The paper designs four different grid systems (i.e., 3.55M, 4.20M, 4.85M and 5.45M) for grid independence. The simulation results of velocity along the Line 1 at 0.3V in Fig. 4. Compared the results of different grid system based on the grid system with the mesh number of 5.45 million, the deviation of the velocity at the cell voltage 0.3 V for the grid number of 0.95 million elements, 1.51 million elements and 2.80 million elements are 16.22%, 8.93% and 2.32%, respectively. We choose the mesh system around 4.85 million elements considering of the calculation cost and the solution accuracy.

In order to validate the numerical model, the simulation results obtained by comparing with the experimental data in terms of polarization curves by Wang et al [46]. The experimental and numerical data are compared in Fig. 5. It is clear that the numerical simulation data are slightly lower than the experimental data, while the result of the low current density is the contrary. However, the simulation results agree with the experimental data reasonably well, thus the model is validated.

4. RESULTS AND DISCUSSION

4.1 Effect of Block Shape in Channel for the PEMFC

4.1.1 Overall output performance

The polarization curves are used as a criterion to evaluate the PEMFC performance. Fig. 6 (a) and (b) displayed current densities and power densities in PEMFC with different blocks. It is found that the curves overlap at low current density. But at the high current density, the PEMFC with blocks in channel performs better than that with conventional channel. The research subjects and basic reference are Cases B-F and Case A, respectively. In Fig. 6, the result of current densities from high to low is Case D > F > E > B > C > A, which is consistent with the change in power densities. In general, the appearance of blocks in channels affects the PEMFC's performance. The electrochemical reaction rate and the amount of reactants that reaches the catalytic layer may be changed.

4.1.2 Temperature

The temperature distribution of membrane on middle plane in *z* direction at 0.3V are shown as Figs. 7. The electrochemical reaction is exothermic and causes the temperature of PEMFC to rise. The value of maximum of Case A (conventional channel) is 388.879K lower than the channels with different blocks. It is worth noting that the temperature region of the neutral plane of the proton membrane on *z*-direction is closer to the front than that the conventional channel. And the area of higher temperature of the PEMFC with blocks in channels (Cases B-F) better than conventional channel (Case A) in the flow direction.

4.1.3 Flow velocity distributions and magnitude

The electrochemical reaction rate is largely determined by the reactant concentration and the fluid flow condition. Fig. 8 show the velocity in the *z* direction about the channels with blocks and conventional channel. Comparing Cases A-F, it is appeared that the *z*-velocity with the blocks structure more than the conventional channel. The mass transfer with the novel block channel will generate forced diffusion effect from channels to GDLs because the blocks will change the flow direction. The reactant concentration involved in the electrochemical reaction is determined by the velocity at which the reactant pass through the diffusion layer. The prompt expulsion of the products can facilitate electrochemical reaction, which is depending on the velocity of the diffusion layer. The balance of two velocities can improve the performance of PEMFC. In Fig.8, the absolute value difference above two velocities with six cases are 0.05435 (Case A), 0.43705 (Case B), 0.63034 (Case C), 0.20995 (Case D), 0.27572 (Case E) and 0.73 (Case F), respectively. It is found that Case D is better shape than other cases because the velocity of reactants are closer to the velocity of products.

4.1.4 Mass transfer within PEMFC

Fig. 9 shows the mass transfer characteristics inside the PEMFC from both reactants and products. And the relatively optimal local O_2 concentration appears in case D as shown Fig. 9 (a). As the reactants involved in the electrochemical reaction are consumed, the O_2 concentration gradually declines along the flow direction. Oxygen concentration and forced diffusion transport are higher in the novel block channel than in the conventional flow channel. It can be concluded that the upper and middle streams are core of the electrochemical reaction (the region with higher oxygen consumption). The diffusion coefficient of liquid water with PEMFC of the novel block channel more than the conventional channel as seen in Fig. 9 (b). The diffusion coefficient of liquid water of PEMFC with the flow channel installed blocks from low to high in turn are Case D < Case B < Case C < Case F < Case E. The reason for the variation of the diffusion coefficient of liquid water is that forced diffusion effect improves the transport of liquid water. For conventional flow channels, the mass transport is in a positive gradient without abrupt change due to the interaction of pressure and concentration fields. There is no forced diffusion effect in the conventional channel so

that the overall diffusion coefficient of the conventional channel is lower than that of the channel using blocks. The forced convection effect is based on the block so that the diffusion coefficient of the channel using block is larger than that of the conventional flow channel. The block will cause the nozzle effect on the channel, reducing the pressure and increasing the speed directly above the block. The diffusion coefficient of water varies with the pressure gradient. In the throat, better water transfer is based on greater velocity.

4.1.5 Pressure drop of the cathode channel and efficiency

The efficiency of any energy device can be defined by the effective (net) outputs and sum inputs. In the section, two concepts of efficiency are defined from the situation of the conversion of chemical energy and the output electrical energy of PEMFC(i.e., η_{LHV} (Electrochemical Efficiency) and η_{OUT} (Net Output Efficiency) [31]).

$$\eta_{OUT} = 1 - \frac{P_{pascal}}{P_{peak}} \tag{20}$$

where P_{pascal} and P_{peak} are the power loss due to pressure drop and the highest power of the PEMFC, respectively. P_{pascal} is satisfied the following equation:

$$P_{pascal} = \left(p_{in} v_{in} - p_{out} v_{out} \right) A \tag{21}$$

where p_{in} and p_{out} are the pressure of the inlet and outlet in channel at cathode; v_{in} and v_{out} are the velocity of the inlet and outlet in channel at cathode, respectively; A is the area of inlet and outlet.

As shown in Fig. 10, the utilization of energy with several novel channel installed blocks and the reference case (conventional flow channel) are compared. In Fig. 10 (a), the minimum increase about the cases of block shape in Electrochemical Efficiency is 8.12% compared with the conventional channel (Case A), and the maximum increase is 15.58% (i.e., Case D).

In Fig. 10 (b), the growth rate of the effective power with PEMFC of the novel block channel from high to low are Case D (15.77%) > Case F (13.61%) > Case E (12.72%) > Case B (11.41%) > Case C (9.71%).

In the discussion and analysis of above several novel block channels, Case D (standard semi-ellipse) shows the best performance. In the following discussion of other performance factors, Case D(standard ellipse) will be the research baseline.

4.2 Effect of Height and Spatial Interval of Blocks on the PEMFC Performance

The effect of block height on the mass transfer and PEMFC's performance is investigated and discussed in this section. The height of blocks are 0.0 (conventional channels), 0.4, 0.5 and 0.6, respectively. The spatial interval of blocks is fixed as 5.0 for the Case D. The output performance of the PEMFC under the different values of height of blocks is shown in Fig. 11 (a) and (b). In general,

the output performance of PEMFCs is obviously improved with the increase of the height value of blocks under the high current density. Fig 12 shows velocity distribution under the different values of block height in *z* direction in flow channels at 0.3V. It can be found that the velocity of reactants and products in and out of the gas diffusion layer is significantly improved with increasing block height, which can improve the forward electrochemical reaction. Fig 13 (a) and (b) show the oxygen concentration and the diffusion coefficient of liquid water along the flow direction, respectively. It is clearly found that the O_2 concentration from high to low in turn are a=0.6 > a=0.5 > a=0.4 > a=0.0 (conventional channel) in the concentrated area of electrochemical reaction. In the vicinity of the blocks, the local oxygen concentration greatly increases and the electrochemical reaction rate is improved. For the diffusion coefficient of liquid water, the curve as a whole tends to increase and then decrease due to electrochemical reaction along the flow direction. The reason is that too much oxygen is consumed and a lot of water is produced in the upstream of channel which causes the decrease of oxygen in downstream. Because of the forced diffusion effect, the forced diffusion transport of liquid water is improved, which makes the whole diffusion coefficient of liquid water decrease with the increase of the value of height of block, especially near the block.

In order to characterize the energy conversion and utilization, electrochemical efficiency and net output efficiency of the PEMFC under the different value of the height of the block are given in Fig. 14 (a) and (b). With the increase of the height, the electrochemical efficiency of the PEMFC from high to low is 17.09% (a=0.6), 15.497% (a=0.5) and 12.72% (a=0.4), respectively. The pressure drop will increase with increasing block height, which can cause the decline of the output power. Compare with the conventional channel, the effective power from high to low is 16.75% (a=0.6), 15.77% (a=0.5) and 13.32% (a=0.4), respectively. However, the effective power is not obvious with the increase of the height of block.

4.3 Effect of Blocks Spatial Interval on the PEMFC Performance

Fig. 15 shows the polarization curves in the different value of spatial interval of blocks used to characterize the PEMFC's performance. However, the current density gradually increases with decreasing blocks spacing at a high current density, which indicates the improved performance of PEMFC. And Fig. 16 shows the velocity at the different spatial intervals of blocks with respect to mass transfer at Line 2 at 0.3V. It is clear that the velocity at the case of p=2.5 is superior to other cases. The small space interval of blocks makes the forced diffusion effect superposition between the blocks, which improves the original flow state. For several other cases, the local velocity (the dorsal sides of the block) is significantly lower than that of the conventional channel, which is disadvantageous for mass transfer in the channel. With the decrease of the value of p, the region

with the minimum velocity significantly declined. The region with the minimum velocity is improved under the mutual influence of forced diffusion effect between blocks.

The oxygen concentration under the different value of spatial interval of blocks at Line 1 at 0.3V are presented in Fig. 17 (a). The O_2 concentration in the case of p=2.5 is higher than in other cases (p=5.0 and p=8.0) due to stronger forced diffusion effect. For the diffusion coefficient of the liquid water in Fig. 17 (b), the diffusion coefficient of liquid water is p=5.0, p=8.0 and p=2.5 from high to low in upstream, and p=8.0, p=5.0 and p=2.5 in the downstream, respectively. The optimal diffusion coefficient is obtained at p=2.5 comparing three cases under the influence of forced diffusion effect for the local diffusion coefficient of liquid water. The forced diffusion effect will reduce the diffusion and improve the velocity of liquid water, which is beneficial for liquid water to pass through the GDL.

Energy conversion and utilization are given in Fig. 18 (a) and (b). As shown in Fig. 18 (a), the electrochemical efficiency of the PEMFC from high to low is 16.95% (p=2.5), 15.49% (p=5.0) and 12.58% (p=8.0), respectively. From the perspective of effective power, the decline of spacing with blocks can cause pressure drop and kinetic energy consumption increase, especially p=2.5 in Fig. 18 (b). The effective power decrease as pressure drop, so that external circuit load can gain less the net power form the PEMFC. However, the net output efficiency of PEMFC fluctuates within the 1%. The effective power will improve with the decline of spatial interval of blocks comparing the conventional channel (p=0). Pressure drop is the most obvious when the spacing of blocks can change, but the effective power is much higher than conventional channel.

5. SUMMARY AND CONCLUSIONS

To research the effects of shape, the height of block (a) and the spatial interval of blocks (p) on the output performance and energy conversion of PEMFC, five different shapes of blocks are presented in the paper. The height of block (a=0.4, a=0.5 and a=0.6) and the spatial interval of blocks (p=2.5, p=5.0 and p=8.0) are considered based on the shape of block. Different parameter variables (temperature, velocity, pressure drop, etc.) were investigated. In this paper, the trend of electrochemical efficiency changes with three research factors(shape, height and spatial interval) is illustrated in **Table 5**, which further summarizes the research work. The following conclusion and the next step work are drawn:

(1) The performance of PEM fuel cell can be significantly improved by installing the blocks in the flow channel. Several novel blocks on the channel can improve the level of mass transport, the O_2 concentration involved in electrochemical reaction proposed in this paper. And the active area of electrochemical reaction is increased and slightly moved forward. Compared with the five cases, the standard semi-ellipse has the best performance and the highest electrochemical efficiency. The

electrochemical conversion efficiency is 15.58% and the effective power is increased by 15.77% comparing the PEMFC of the conventional channel.

(2) Based on the above optimal structure -- standard semi-ellipse, the effect of height of block on the PEMFC's performance is investigated. It draws a conclusion that the concentration polarization of PEMFC is decreased due to forced diffusion effect with the increase of the height of block. The reactants concentration is improved, which can enhance the electrochemical efficiency and the effective power. The best one of the three value of height of block (a=0.4, a=0.5 and a=0.6) is a=0.6. And its electrochemical conversion efficiency is 17.09% and the effective power is increased by 16.75%.

(3) The spatial interval of blocks is the last aspect of the paper building on the standard ellipse. The output performance of PEMFC will increase with the decrease of spatial interval of blocks. The case of p=2.5 is the best one compared with other two cases (p=5.0 and p=8.0). The smaller spatial interval of blocks can improve the mass transport in the PEMFC and prevent the product accumulation caused by the low velocity. In addition, as the spatial interval of blocks increases, the interaction of the forced diffusion effect between blocks will improve the transport of reactants and products as well as concentration distribution and flow state. The case with the best performance is p=2.5. The electrochemical conversion efficiency is 16.95% and the effective power is increased by 16.83%.

(4) In this study, some relatively good conclusions were drawn. However, there are some shortcomings and the next step of this technology planning. **a)**. The instructive conclusions are based on a number of assumptions. The conclusions of this study will likely change when considering the contact resistance between layers, especially the contact between GDL and current collector. **b)**. For the effect of parameters (i.e., height and spatial interval) on the performance of PEMFC, the relatively few cases were selected. It is possible to find a local optimum rather than a global optimum based on three factors. **c)**. Water management is very important for the performance and durability of PEMFC. The water transport of the catalytic layer and the gas diffusion layer are the same, but it is not sufficiently considered for the channels. The water transfer equation may not be applicable and further experimental studies are needed for the stack. The next step of the flow channel adding block should focus on the study of water management.

ACKNOWLEDGEMENTS

This work was sponsored by the National 111 Project under Grant no. B18041. Prof. Meng Ni would thank the grant (Project Number: PolyU 152214/17E) from Research Grant Council, University Grants Committee, Hong Kong SAR.

REFERENCES

[1] Garche J, Jörissen L. *Handbook of Fuel Cells – Fundamentals, Technology and Applications*. New York: Wiley; 2010.

[2] Arato E, Costa P. Transport mechanisms and voltage losses in PEMFC membranes and at electrodes: A discussion of open-circuit irreversibility. *Journal of Power Sources* 2006;159:861-868.

[3] Paul DK, Fraser A, Karan K. Towards the understanding of proton conduction mechanism in PEMFC catalyst layer: Conductivity of adsorbed Nafion films. *Electrochemistry Communications* 2011;13:774-777.

[4] Taner T. Alternative Energy of the Future: A Technical Note of PEM Fuel Cell Water Management. *Fundamentals of Renewable Energy and Applications* 2015;5(3):1000163.

[5] Taner T. The Micro-scale Modeling by Experimental Study in PEM Fuel Cell. *Journal of Thermal Engineering* 2017;3(6), Special Issue 6 :1515-1526.

[6] Pasaogullari U, Wang CY. Two-phase transport and the role of micro-porous layer in polymer electrolyte fuel cells. *Electrochimica Acta* 2004;49:4359-4369.

[7] Taner T. Energy and exergy analyze of PEM fuel cell: A case study of modeling and simulations. *Energy* 2018;143:284-294.

[8] Taner T. A flow channel with Nafion membrane material design of PEM fuel cell. *Journal of Thermal Engineering* 2019;5(5):456-468.

[9] Zhao J, Ozden A, Shahgaldi S, Alaefour IE, Li XG, Hamdullahpur F. Effect of Pt loading and catalyst type on the pore structure of porous electrodes in polymer electrolyte membrane (PEM) fuel cells. *Energy* 2018;150:69-76.

[10] Beltrán-Gastélum M, Salazar-Gastélum MI, Flores-Hernández JR, Botte GG, Pérez-Sicairos S, Romero-Castañon T, Reynoso-Soto E, Félix-Navarro RM. Pt-Au nanoparticles on graphene for oxygen reduction reaction: Stability and performance on proton exchange membrane fuel cell. *Energy* 2019;181:1225-1234.

[11] Siegel NP, Ellis MW, Nelson DJ, von Spakovsky MR. Single domain PEMFC model based on agglomerate catalyst geometry. *Journal of Power Sources* 2003;115:81-89.

[12] Sui PC, Zhu X, Djilali N. Modeling of PEM fuel cell catalyst layers: status and outlook. *Electrochemical Energy Reviews* 2019.

[13] Taner T, Naqvi SAH, Ozkaymak M. Techno-economic Analysis of a More Efficient Hydrogen Generation System Prototype: A Case Study of PEM Electrolyzer with Cr-C Coated SS304 Bipolar Plates. *Fuel Cells* 2019;19(1):19-26.

[14] Wilberforce T, Ijaodola O, Ogungbemi E, Khatib FN, Leslie T, El-Hassan Z, Thomposon J, Olabi AG. Technical evaluation of proton exchange membrane (PEM) fuel cell performance –

A review of the effects of bipolar plates coating. *Renewable and Sustainable Energy Reviews* 2019;113:109286.

[15] Wilberforce T, Khatib FN, Ijaodola OS, Ogungbemi E, El-Hassan Z, Durrant A, Thompson J, Olabi AG. Numerical modelling and CFD simulation of a polymer electrolyte membrane (PEM) fuel cell flow channel using an open pore cellular foam material. *Science of the Total Environment* 2019;678:728-740.

[16] Ashrafi M, Kanani H, Shams M. Numerical and experimental study of two-phase flow uniformity in channels of parallel PEM fuel cells with modified Z-type flow-fields. *Energy* 2018;147:317-328.

[17] Havaej P. A numerical investigation of the performance of Polymer Electrolyte Membrane fuel cell with the converging-diverging flow field using two-phase flow modeling. *Energy* 2019;182:656-672.

[18] Wilberforce T, El-Hassan Z, Khatib FN, Makky AA, Mooney J, Barouaji A, Carton JG, Olabi AG. Development of Bi-polar plate design of PEM fuel cell using CFD techniques. *ScienceDirect* 2017;42:25663-25685.

[19] Iranzo A, Arredondo CH, Kannan AM, Rosa F. Biomimetic flow fields for proton exchange membrane fuel cells: A review of design trends. *Energy* 2020;190:116435.

[20] Wilberforce T, El-Hassan Z, Ogungbemi E, Ijaodola O, Khatib FN, Durrant A, Thompson J, Baroutaji A, Olabi AG. A comprehensive study of the effect of bipolar plate (BP) geometry design on the performance of proton exchange membrane (PEM) fuel cells. *Renewable and Sustainable Energy Reviews* 2019;111:236-260.

[21] Li SA, Yuan JL, Andersson M, Xie GN, Sundén B. Influence of anisotropic gas diffusion layers on transport phenomena in a proton exchange membrane fuel cell. *International Journal of Energy Research* 2017; 41:2034-2050.

[22] Yin Y, Wang XF, Zhang JF, Shangguan X, Qin YZ. Influence of sloping baffle plates on the mass transport and performance of PEMFC. *International Journal of Energy Research* 2018;43:2643-2655.

[23] Perng SW, Wu HW. Non-isothermal transport phenomenon and cell performance of a cathodic PEM fuel cell with a baffle plate in a tapered channel. *Applied Energy* 2011; 88:52-67.

[24] Cai GC, Liang YM, Liu ZC, Liu W. Design and optimization of bio-inspired wave-like channel for a PEM fuel cell applying genetic algorithm. *Energy* 2020;192:116670.

[25] Yi JS, Nguyen TV. An along-the-channel model for proton exchange membrane fuel cells. *Journal of The Electrochemical Society* 1998; 145(4):1149-1159.

[26] Hosseini M, Afrouzi HH, Arasteh H, Toghraie D. Energy analysis of a proton exchange membrane fuel cell (PEMFC) with an open-ended anode using agglomerate model: A CFD study. *Energy* 2019;188:116090.

[27] Yang XG, Ye Q, Cheng P. Matching of water and temperature fields in proton exchange membrane fuel cells with non-uniform distributions. *International Journal of Hydrogen Energy* 2011;36:12524-12537.

[28] Pasaogullari U, Mukherjee PP, Wang CY, Chen KS. Anisotropic heat and water transport in a PEFC cathode gas diffusion layer. *Journal of The Electrochemical Society* 2007; 154(8):B823-B834.

[29] Berning T, Lu DM, Djilali N. Three-dimensional numerical analysis of transport phenomena in a PEM fuel cell. *Journal of Power Sources* 2002; 106:284-294.

[30] Galitskaya EA, Gerasimova EV, Dobrovol'skii YA, Don GA, Afanas'ev AS, Levchenko AV, Sivak AV, Sinitsyn VV. Pulsed activation of a fuel cell on the basis of a proton-exchange polymer membrane. *Technical Physics Letters* 2018;44(7):570-573.

[31] Cai YH, Fang Z, Chen B, Yang TQ, Tu ZK. Numerical study on a noval 3D cathode flow field and evaluation criteria for the PEM fuel design. *Energy* 2018; 161:28-37.

[32] Buchanan F. *PEM Fuel Cells: Theory, Performance and Applications*. New York: NOVA; 2015.

[33] Wu HW, Shih GJ, Chen YB. Effect of operational parameters on transport and performance of a PEM fuel cell with the best protrusive gas diffusion layer arrangement. *Applied Energy* 2018; 220:47-58.

[34] Nam JH, Karviany M. Effective diffusivity and water-saturation distribution in single- and two-layer PEMFC diffusion medium. *International Journal of Heat and Mass Transfer* 2003; 46(24):4595-4611.

[35] Springer TE, Zawodzinski TA, Gottesfeld S. Polymer electrolyte fuel cell model. *Journal of the Electrochemical Society* 1991; 138(8):2334-2342.

[36] Barbir F. *PEM Fuel Cells: Theory and Practice-2nd edition*. New York: Elsevier; 2013.

[37] Wang L, Husar A, Zhou TH, Liu HT. A parametric study of PEM fuel cell performance. *International Journal of Hydrogen Energy* 2003; 28:1263-1272.

Table 1 Geometric modeling parameters and operating conditions.

	Items	Parameters	Value	Unit
Parameters of the single PEMFC	Total thickness of the single PEMFC	H_s	3.47	mm
	Thickness of current collector (CC)	H_{cc}	1.5	mm
	Thickness of gas diffusion layer (GDL)	H_{gd}	0.2	mm
	Thickness of catalyst layer (CL)	H_{cl}	0.01	mm
	Thickness of membrane	H_m	0.05	mm
Parameters of the computational domain	Width of the computational domain	W_{cd}	2.0	mm
	Length of the computational domain	L_{cd}	50	mm
	Total height the computational domain	H_{cd}	1.0	mm
Parameters of the flow channel	Width of the flow channel	W_{ch}	1.0	mm
	Depth of the flow channel	H_{ch}	1.0	mm
	Length of the flow channel	L_{ch}	50	mm
Operating condition	Cell temperature	T	353.15	K
	Relative humidification in anode inlet	RH_a	100%	–
	Relative humidification in cathode inlet	RH_c	100%	–
	Anode pressure	p_a	1.0	atm
	Cathode pressure	p_c	1.0	atm

Table 2 The main research factors are about different shapes of blocks

Factors	Cases	*a* (mm)	*p* (mm)
Shape	A B C D E F	0.5	5
The height of block (*a*)	Optimal{A,B,C,D,E,F}	0.4, 0.5, 0.6	5
The spatial interval of blocks (*p*)	Optimal{A,B,C,D,E,F}	0.5	2.5, 5.0 ,8.0

Table 3 Source terms in the conservation equations of mass, momentum, energy, species and charge.

	Expression	Description	Units
S_M	$S_M = S_{H_2} + S_{O_2} + S_{H_2O}$	ACL,AGDL, CCL and CGDL	$\mathrm{kg/m^3 \cdot s}$
S_{MOM}	$S_{MOM} = -\frac{\mu}{K}\vec{u}$	ACL,AGDL, CCL and CGDL	$\mathrm{kg/m^2 \cdot s^2}$
S_E	$S_E = h_{react} - i_{an,cat}\eta_{an,cat} + I^2 R_{ohm} + h_L$	Membrane, ACL, AGDL, CCL and CGDL	$\mathrm{W/m^3}$
S_{H_2}	$S_{H_2} = -\frac{M_{H_2}}{2F} i_{an}$	ACL	$\mathrm{kg/m^3 \cdot s}$
S_{O_2}	$S_{O_2} = -\frac{M_{O_2}}{4F} i_{ca}$	CCL	$\mathrm{kg/m^3 \cdot s}$
S_{H_2O}	$S_{H_2O} = \frac{M_{H_2O}}{2F} i_{ca}$	ACL and CCL	$\mathrm{kg/m^3 \cdot s}$
S_S	$S_S = -i_{an}$	ACL	$\mathrm{A/m^3}$
S_m	$S_m = +i_{an}$	ACL	$\mathrm{A/m^3}$
S_S	$S_S = +i_{ca}$	CCL	$\mathrm{A/m^3}$
S_m	$S_m = -i_{ca}$	CCL	$\mathrm{A/m^3}$

Table 4 Physical parameters used in numerical simulations.

Parameters	Symbol	Value	Unit	References
Dry membrane density	ρ_m	2000	kg/cm^3	Li et al [21]
Dry membrane equivalent weight	ME_m	1100	kg/cm^3	Li et al [21]
Molar volume of dry membrane	V_m	5.5×10^{-4}	kg/cm^3	Li et al [21]
Porosity of CLs	ε_{CL}	0.6	−	Li et al [21]
Porosity of GDLs	ε_{GDL}	0.35	−	Li et al [21]
Contact angel	θ_c	120	−	Yi and Nguyen [25]
Surface tension	σ	0.0625	N/m	Li et al [21]
Transfer coefficient in anode	α_a	0.5	−	Hosseini et al [26]
Transfer coefficient in cathode	α_c	1	−	Hosseini et al [26]
Stoichiometry ratio in anode side	ξ_a	1	−	assume
Stoichiometry ratio in cathode side	ξ_c	1	−	assume
Ref exchange current density in anode	i_a	1	A/cm^3	Li et al [21]
Ref exchange current density in cathode	i_c	1	A/cm^3	Li et al [21]
Ref concentration in anode	$c_{H_2}^{ref}$	546.5	mol/m^3	Li et al [21]
Ref concentration in cathode	$c_{O_2}^{ref}$	3.39	mol/m^3	Li et al [21]
Thermal conductivity of membrane	kt_m	0.25	$W/m\cdot K$	Yang et al [27]
Thermal conductivity of GDLs	$kt_{gd,x}/kt_{gd,z}$	1.7/21	$W/m\cdot K$	Pasaogullari et al [28]
Thermal conductivity of CLs	kt_{cl}	0.3	$W/m\cdot K$	Yang et al [27]
Thermal conductivity of CCs	kt_{cc}	100	$W/m\cdot K$	Yang et al [27]
Electrical conductivity of GDLs	σ_{gd}	5000	S/m	Yang et al [27]
Electrical conductivity of CLs	σ_{cl}	2000	S/m	Yang et al [27]
Electrical conductivity of CCs	σ_{cc}	20000	S/m	Yang et al [27]
Diffusion coefficient of hydrogen	D_{H_2}	9.15×10^{-5}	m^2/s	Berning et al [29]
Diffusion coefficient of oxygen	D_{O_2}	2.2×10^{-5}	m^2/s	Berning et al [29]
Diffusion coefficient of water vapor	D_{H_2O}	2.56×10^{-5}	m^2/s	Berning et al [29]
Open circuit voltage	V_{OCV}	0.95	V	Galitskaya et al [30]

Table 5 The trend of electrochemical efficiency with research factors.

Cases	Height of blocks (a)	a=0.0 → a=0.4 → a=0.5 → a=0.6
	Conventional channel Thin semi-ellipse Semi-circle Special-shape profile Half regular hexagon Standard semi-ellipse	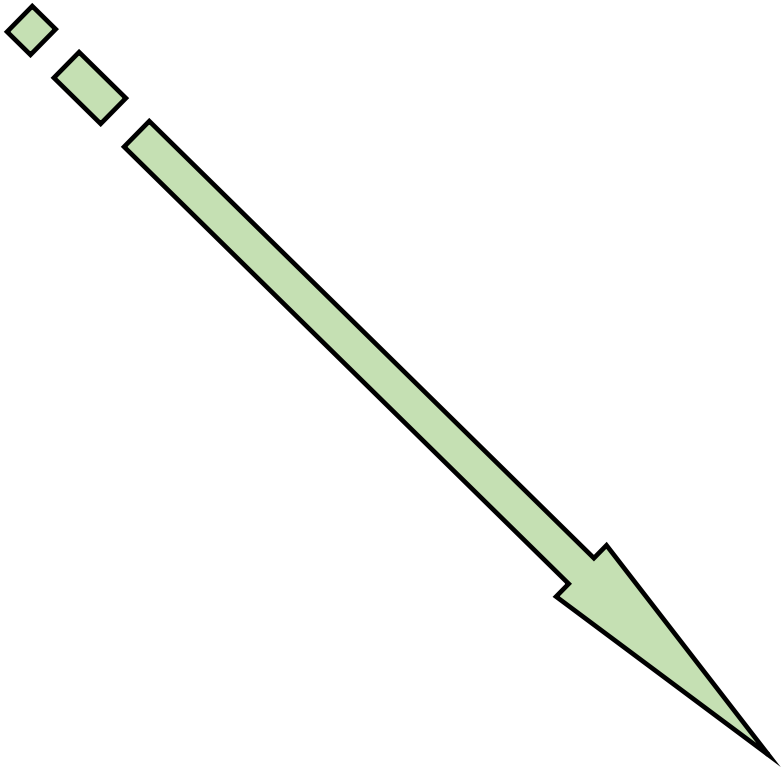
	Interval between two neighbouring blocks (p)	p=0.0 → p=8.0 → p=5.0 → p=2.5

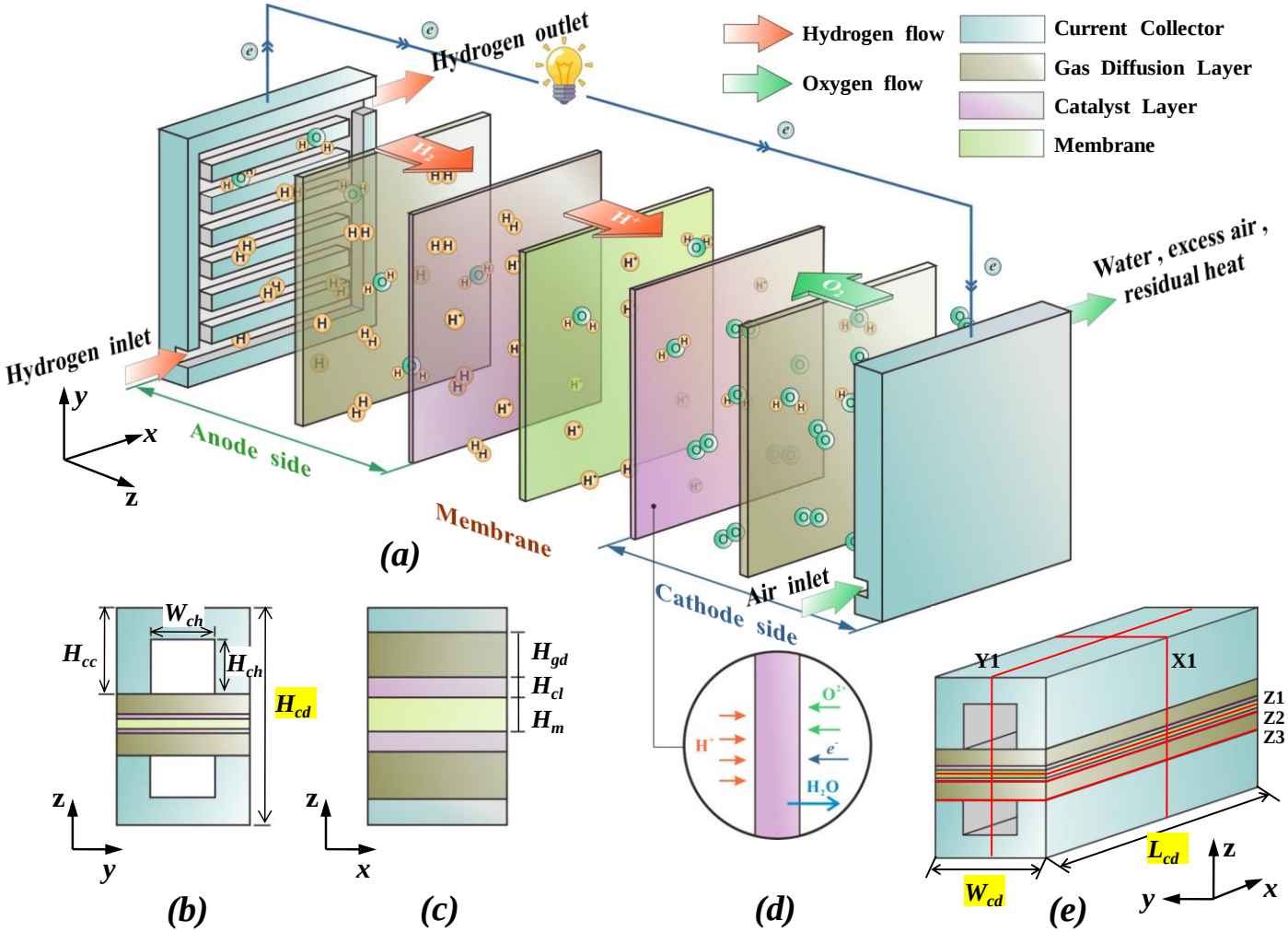

Fig.1 Schematic of PEMFC system with conventional flow channels. (a) A sketch of 3D parallel flow field system; (b) Descriptions of geometric parameters in inlet about anode; (c) Geometric dimension of membrane electrode assembly; (d) The flow of reactants in cathode CL; (e) Auxiliary line and surfaces in the research.

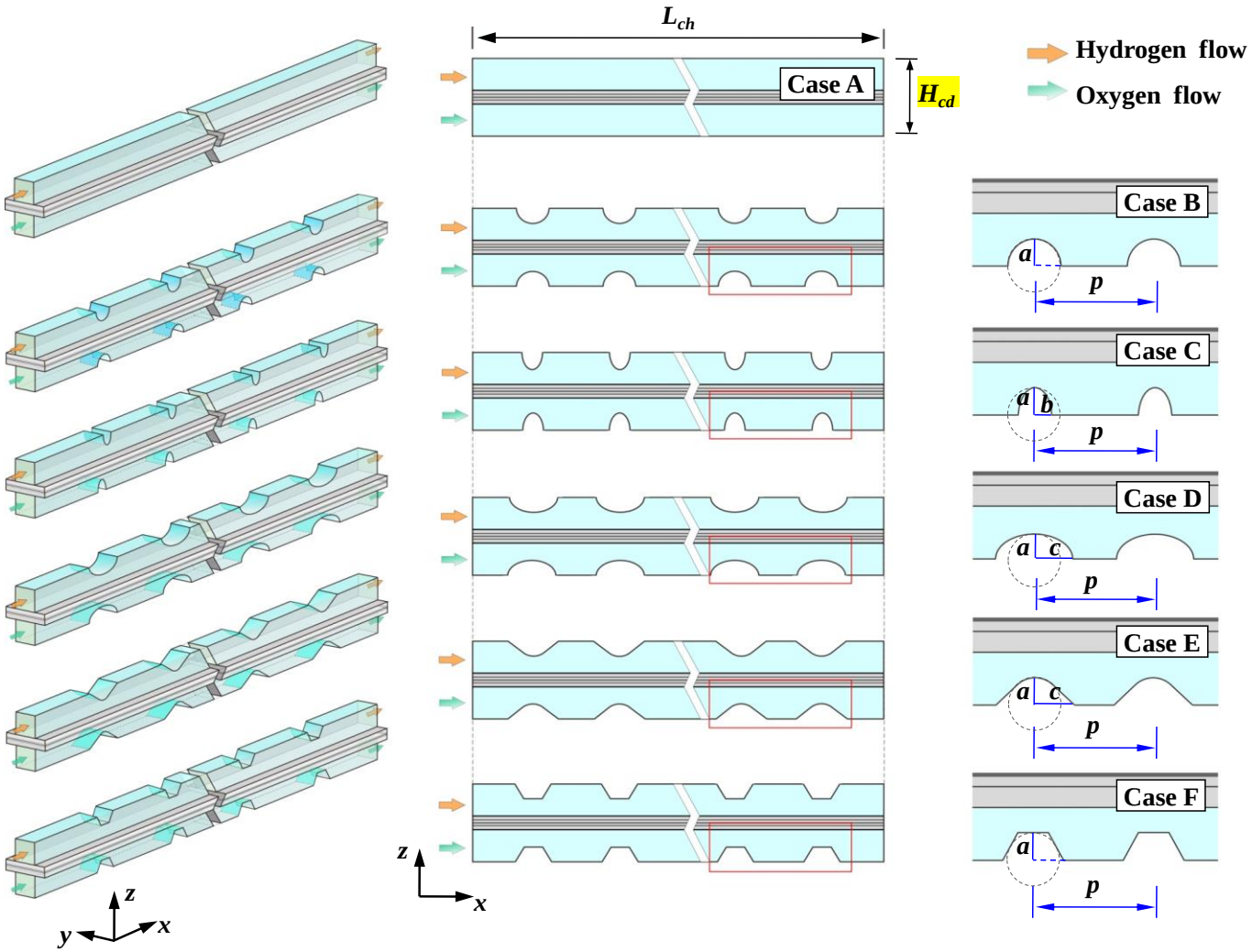

Fig.2 Sketch of six channel with the various shapes of baffle (Case A: conventional; Cases B-F: Block) and expression of the main design parameters for the novel blocks.

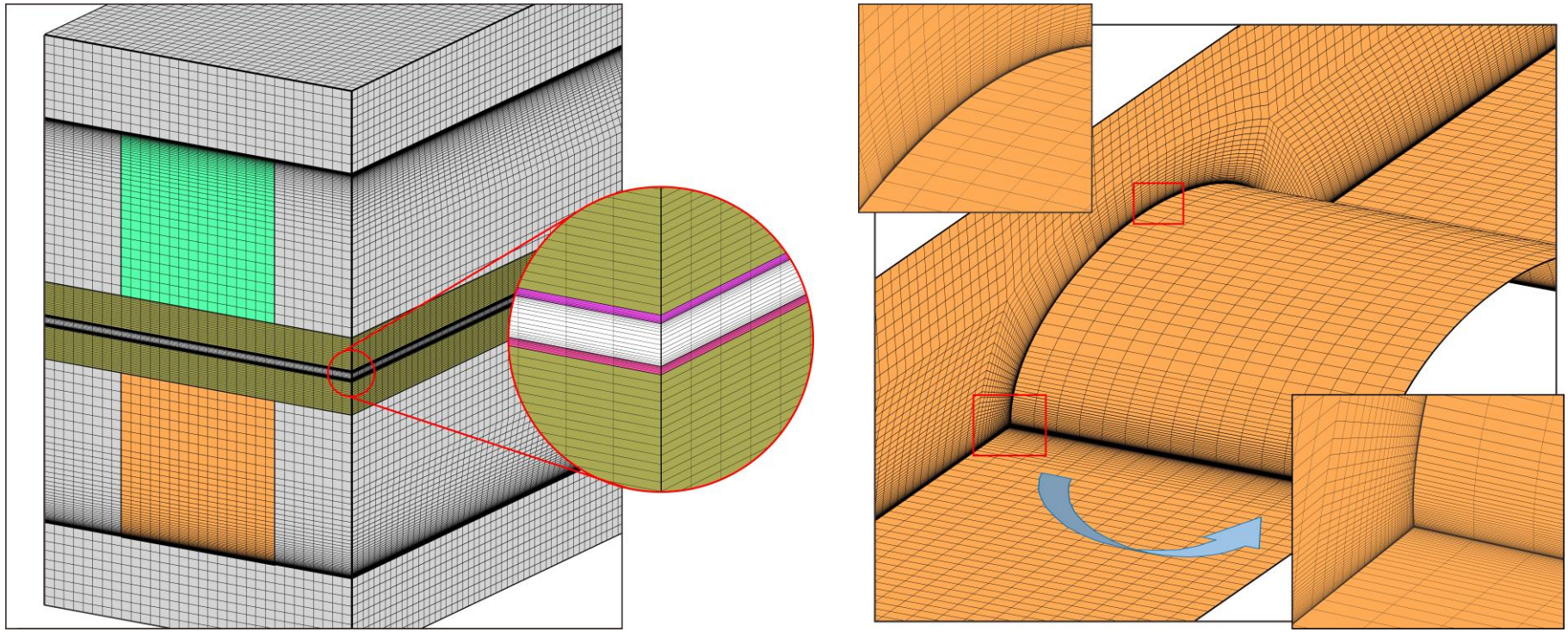

Fig.3 Structured mesh in the presented simulations (take Case D as an example). (a) the global mesh of the single computational domain and the local mesh near membrane electrode assembly; (b) the local mesh near the baffle in the cathode channel.

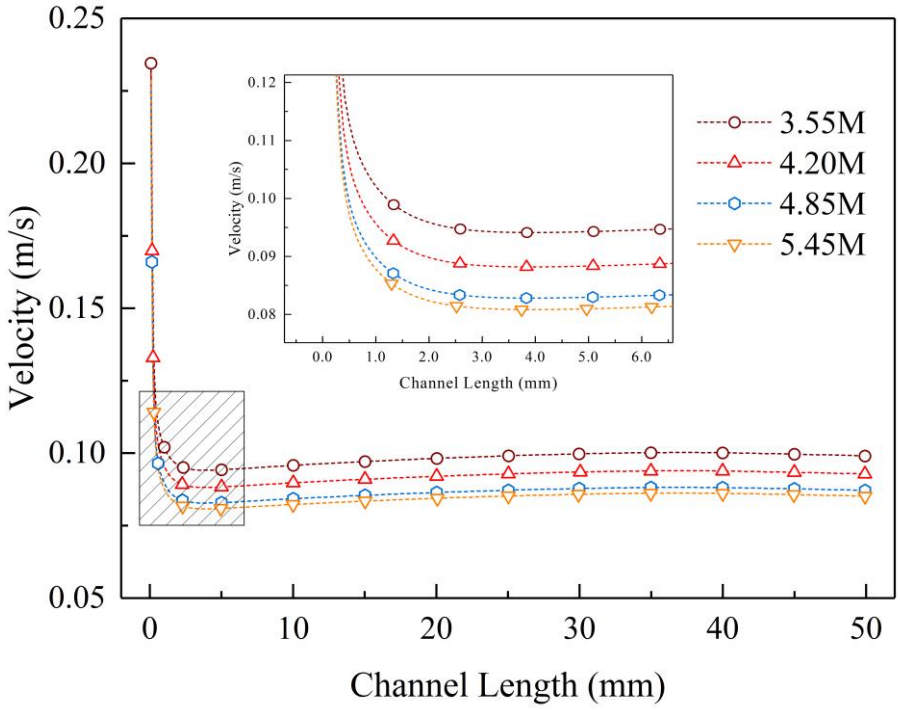

Fig.4 The oxygen flow velocity magnitude comparison along Line 2 in cathode at 0.3V under four mesh system. (Case A; m_{an} = 1200 sccm, m_{ca}= 2200 sccm).

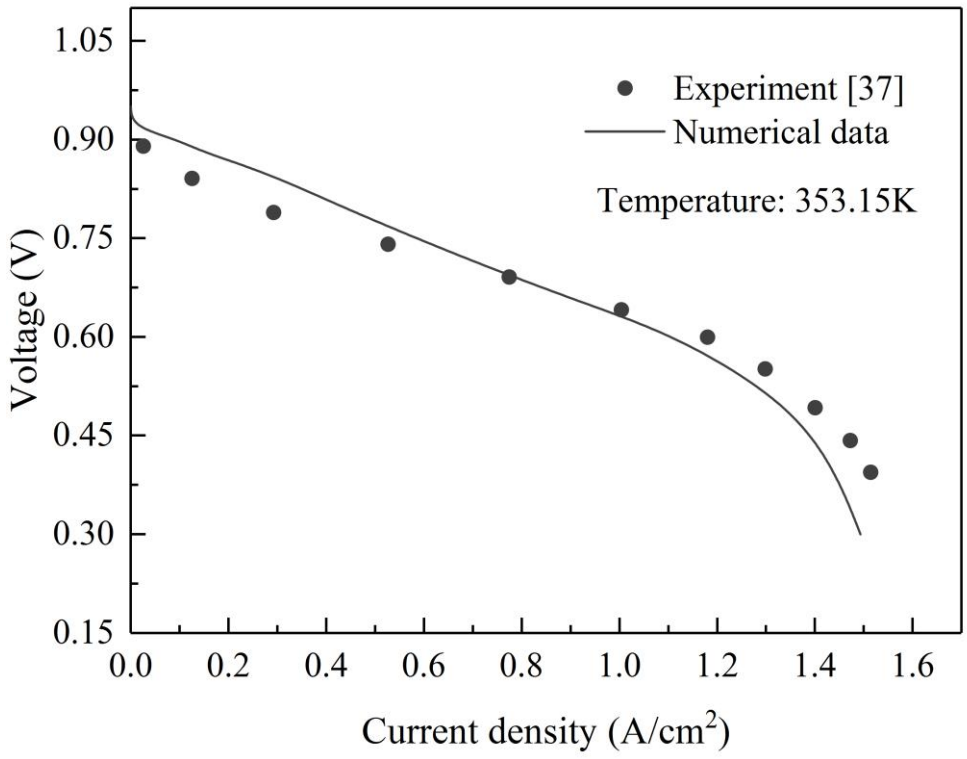

Fig.5 Model validation about the simulation results by comparing with polarization curves obtained from the experimental data (Wang et al. [37]). (m_{an}= 1200 sccm, m_{ca}= 2200 sccm).

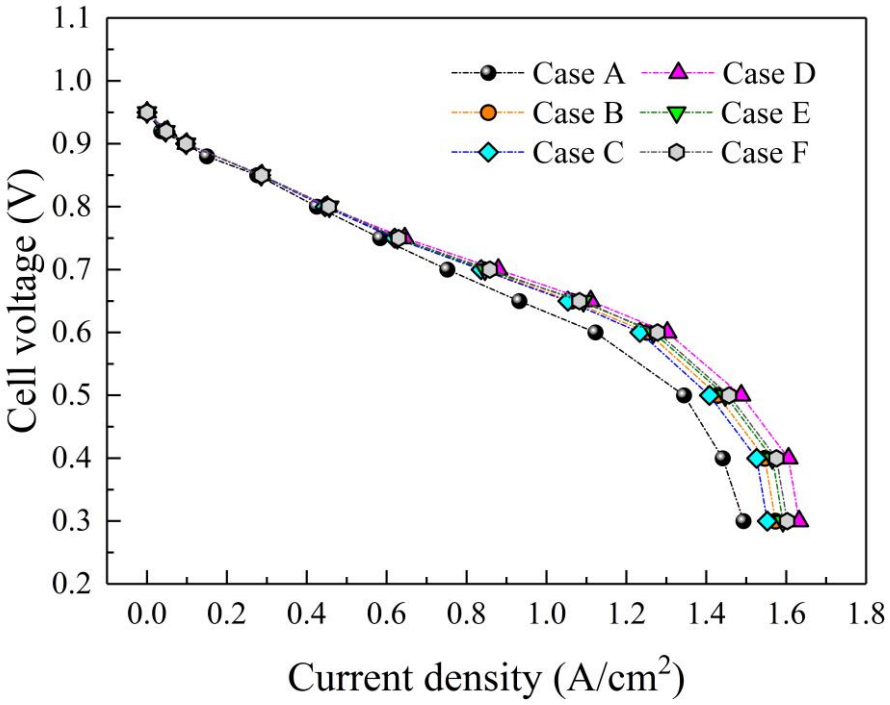

(a)

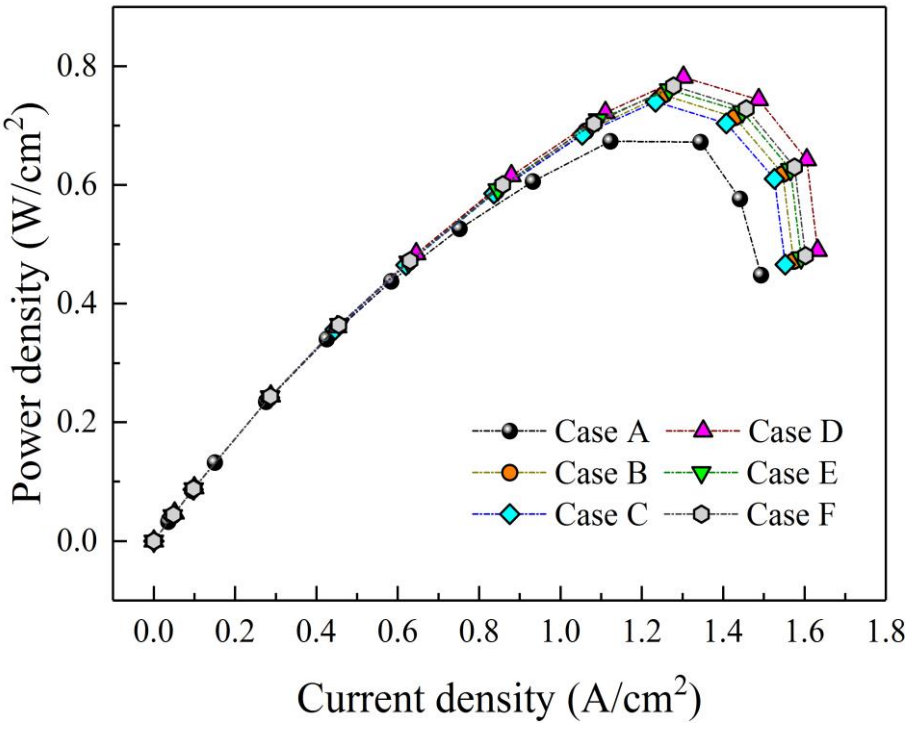

(b)

Fig.6 PEMFC output performance under the different block shapes in channel. (a) Polarization curves; (b) Power curves

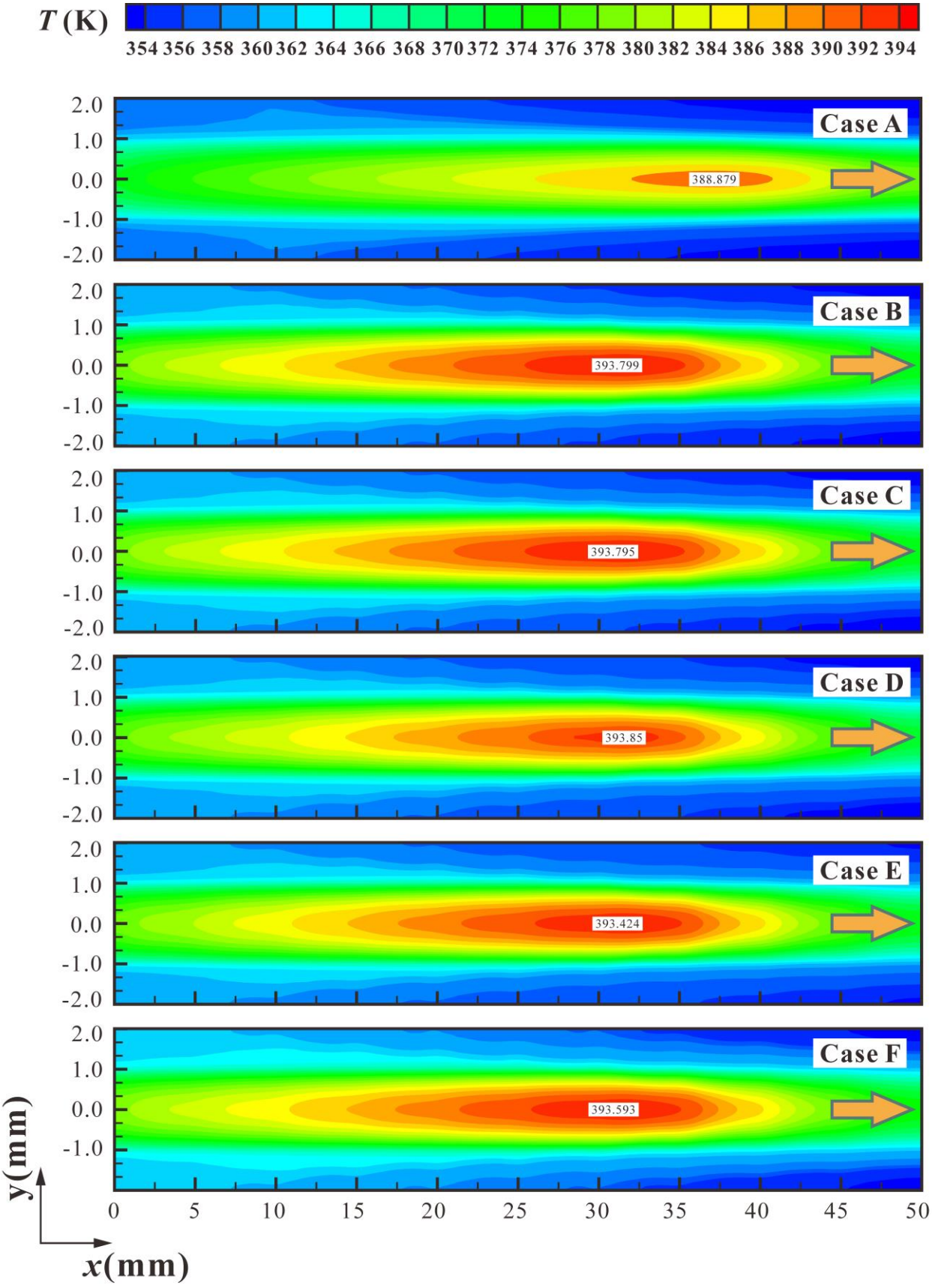

Fig.7 Temperature about different block shapes on mid plane in *z* axis direction of membrane at 0.3V(Plane Z1 in Fig. 1 (c), *z*= 0 mm).

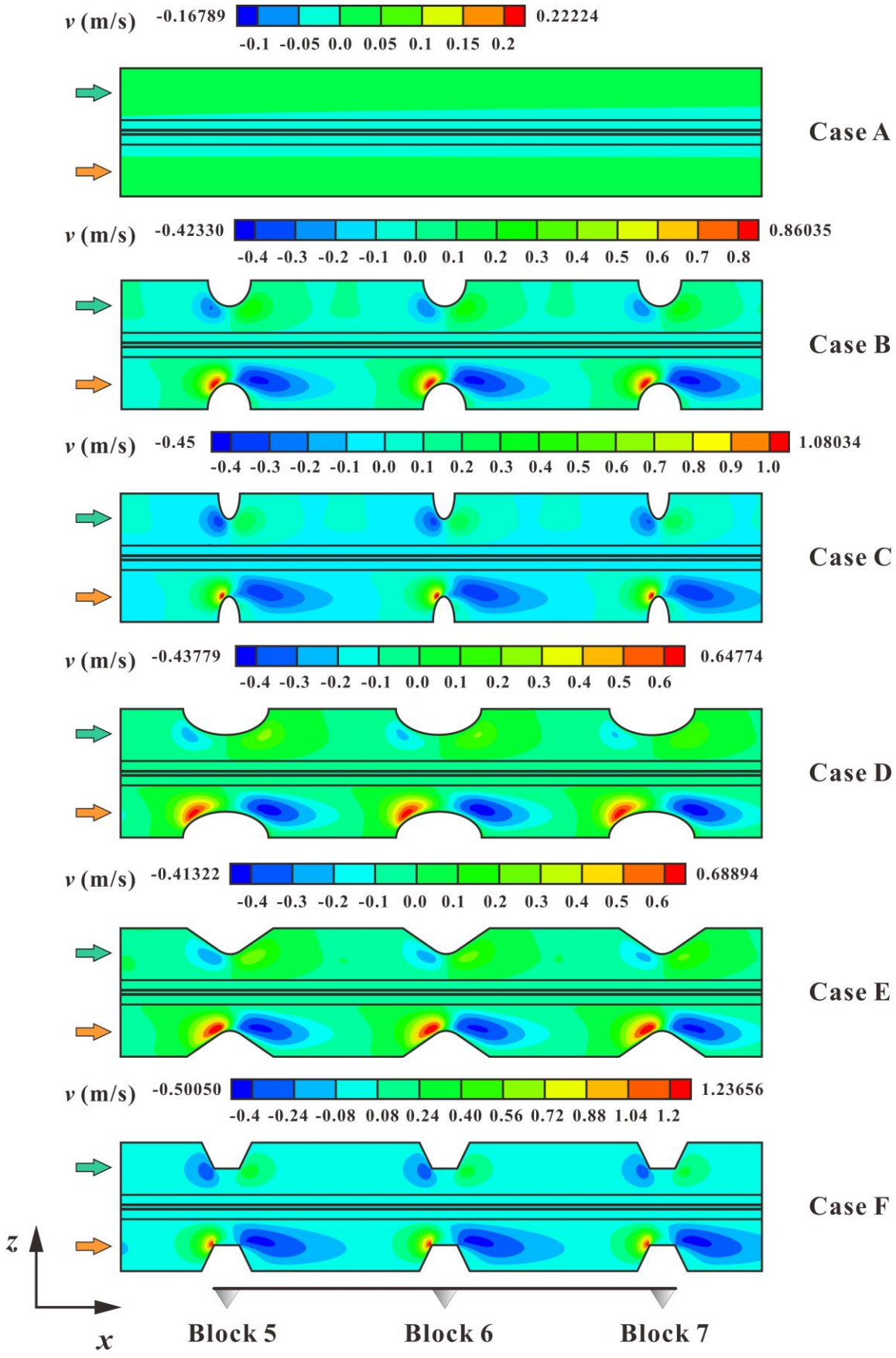

Fig.8 Velocity distribution in *z* direction about different block shapes with flow channels on plane Y1 at 0.3V(The collector plate is omitted, *y*=0mm).

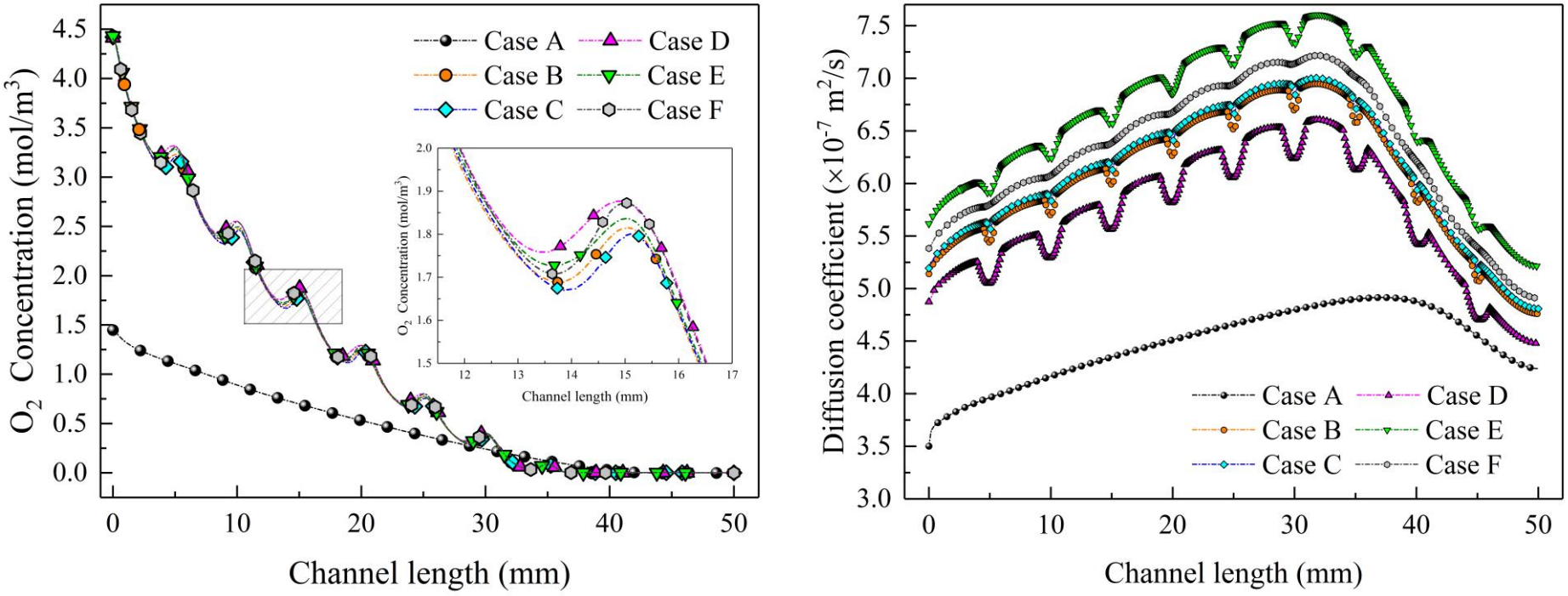

Fig.9 Mass transfer characteristics about different block shapes. (a) Oxygen concentration at Line 1 at 0.3V; (b) Diffusion coefficient of liquid water at Line 2 at 0.3V.

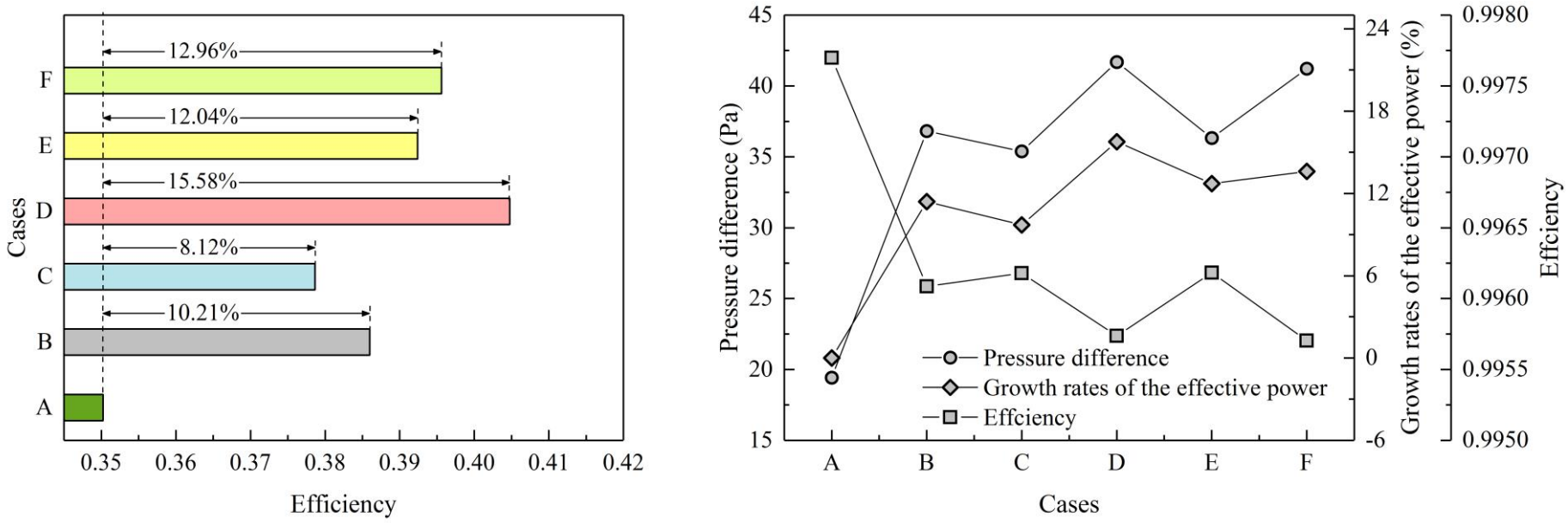

Fig.10 Conversion and loss of electrochemical energy of PEMFC with different novel block shapes. (a) Comparison of electrochemical efficiency; (b) Comprehensive comparison about loss of energy

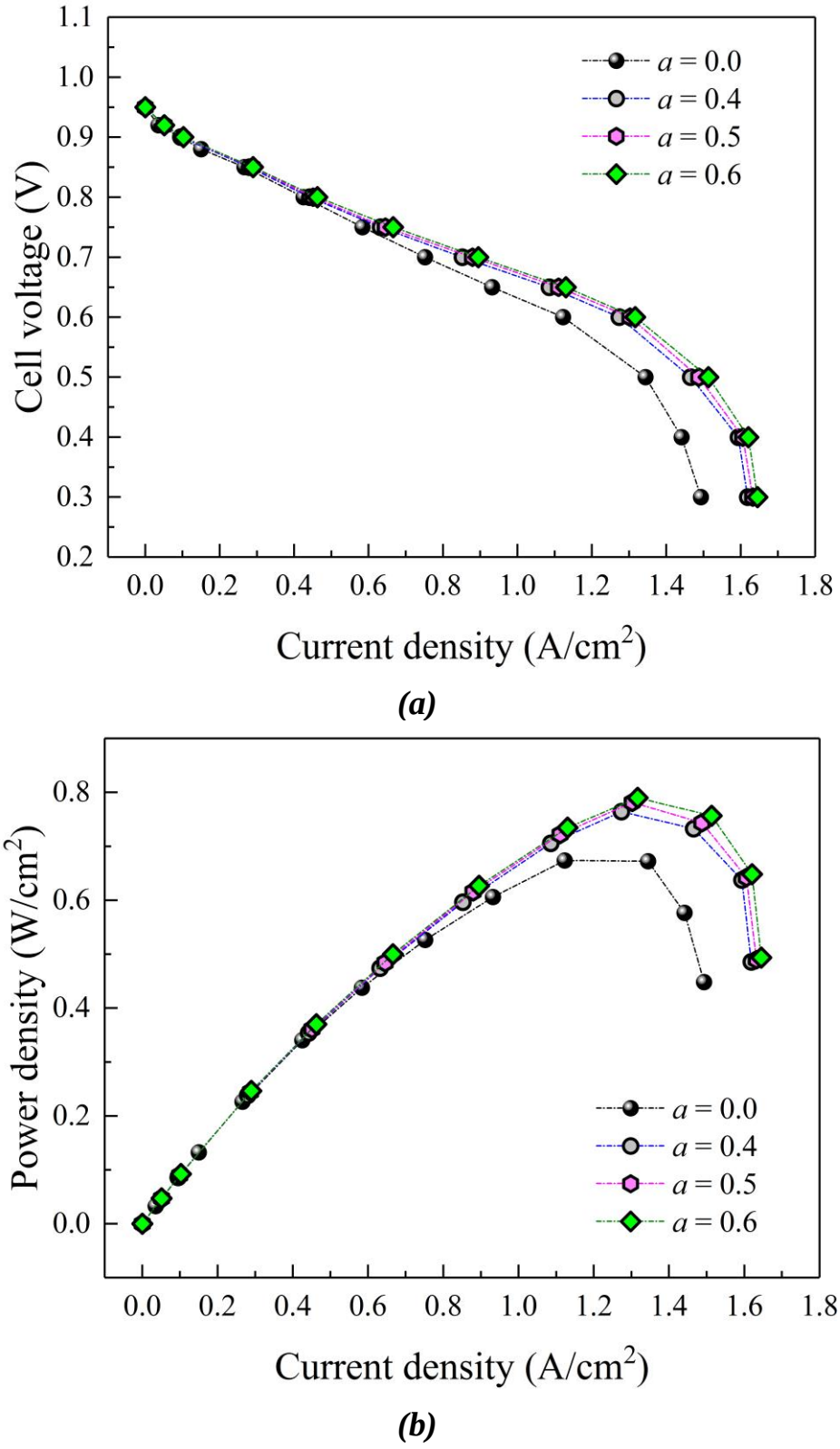

Fig.11 The output performance of the PEMFC under the different value of height of blocks in channel. (a) Polarization curves; (b) Power curves.(Case D).

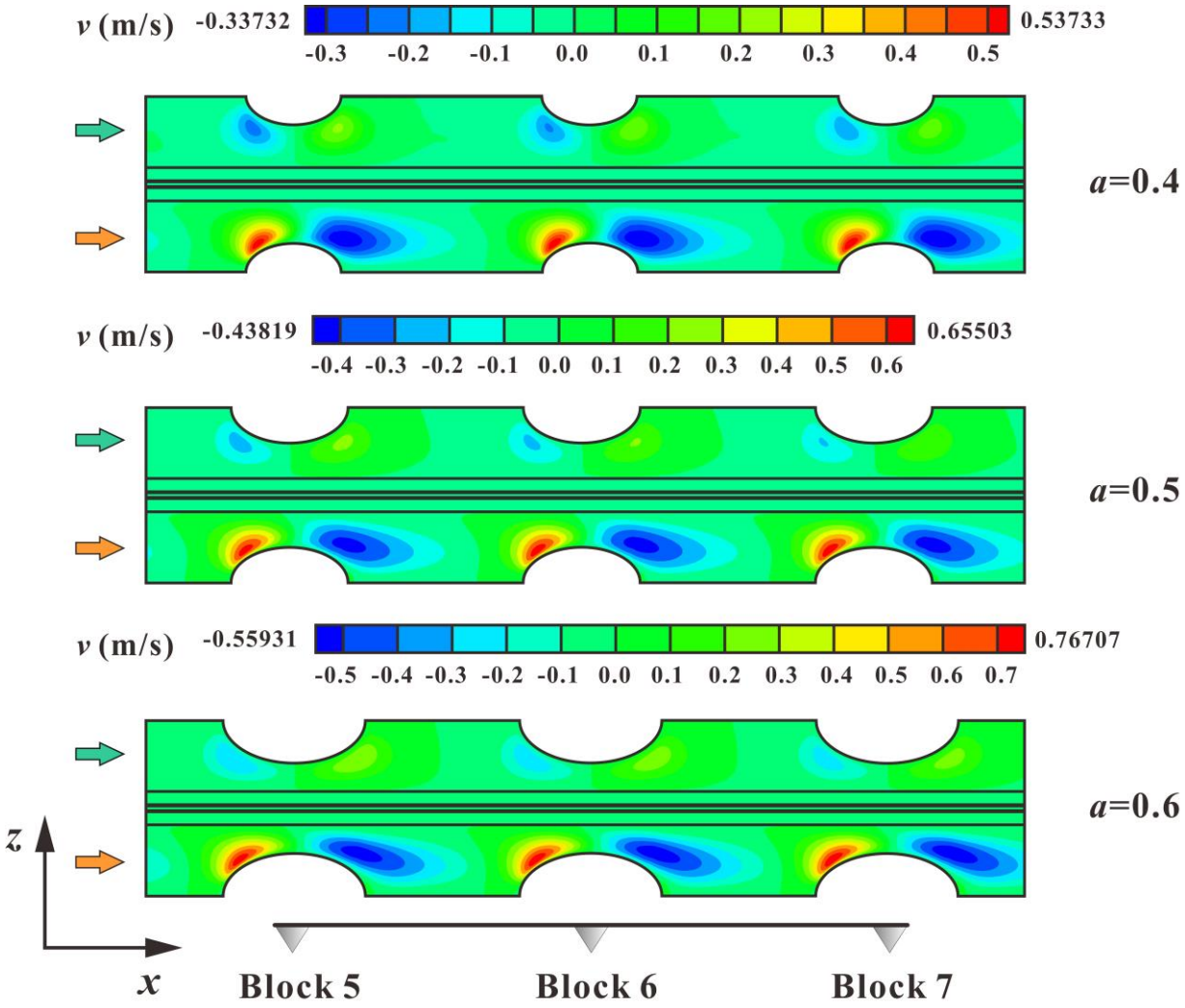

Fig.12 Velocity distribution in z direction under the different value of height of blocks (flow direction) in flow channels on plane Y1 at 0.3V(The collector plate is omitted, *y*=0mm; Case D).

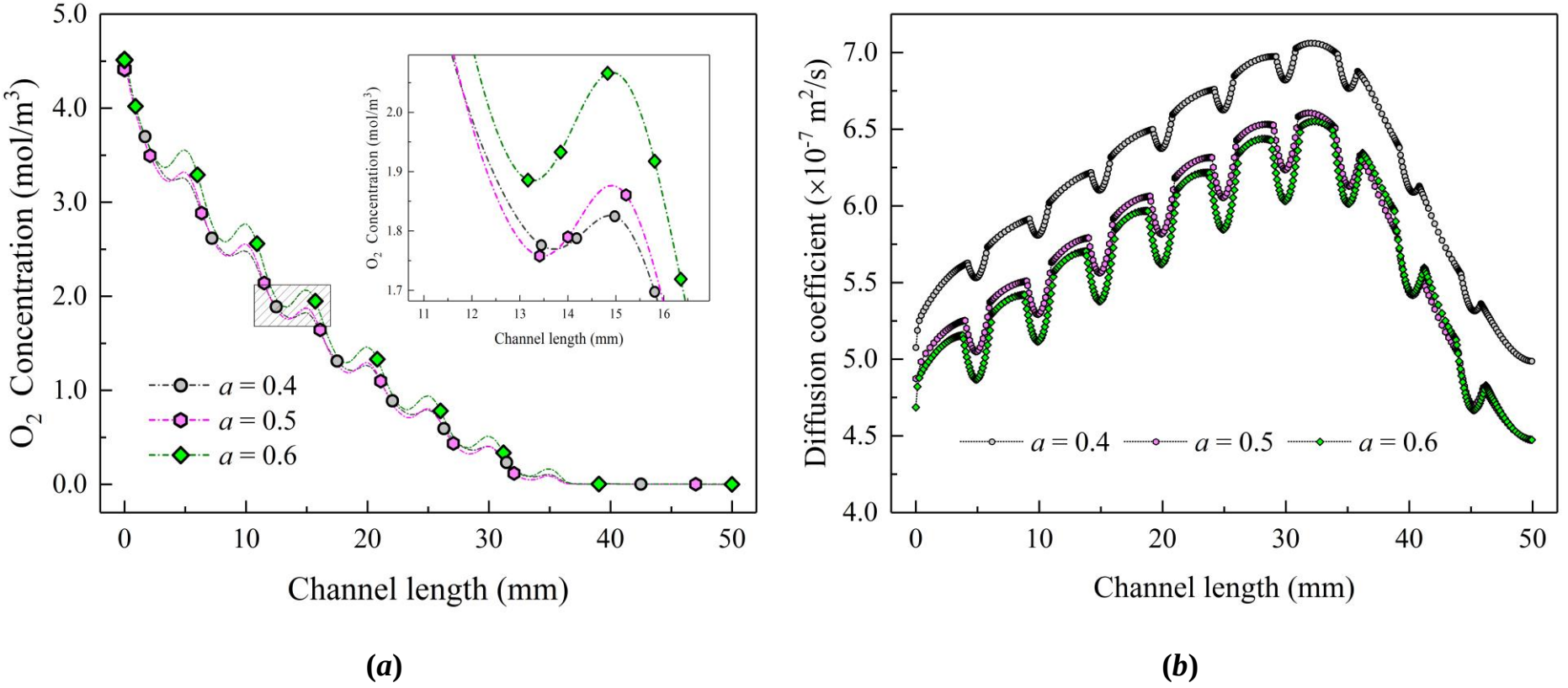

Fig.13 Mass transfer characteristics under the different value of height of blocks(Case D). (a) Oxygen concentration at Line 1 at 0.3V; (b) Diffusion coefficient of liquid water at Line 2 at 0.3V.

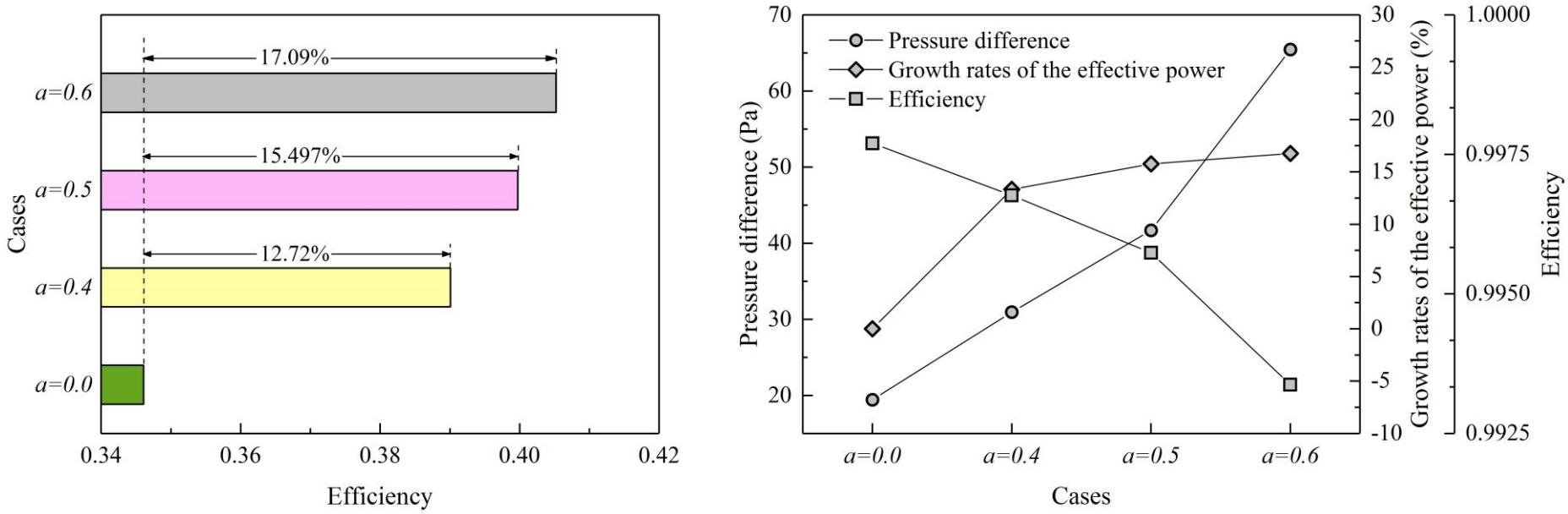

Fig.14 Conversion and loss of electrochemical energy of PEMFC under the different value of height of blocks (Case D). (a) Comparison of electrochemical efficiency; (b) Comprehensive comparison about loss of energy.

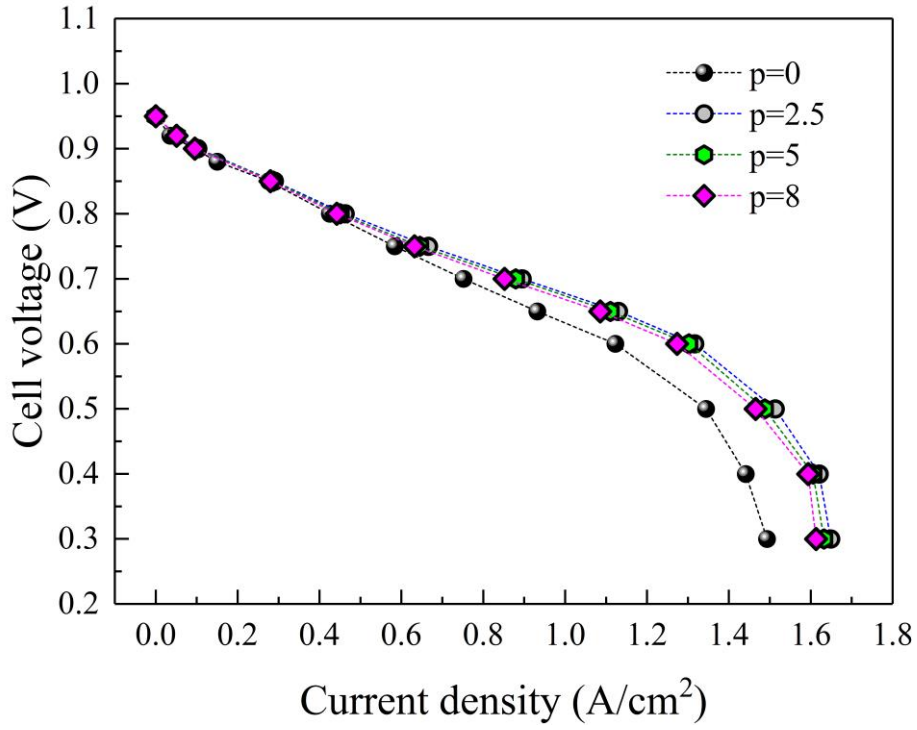

(a)

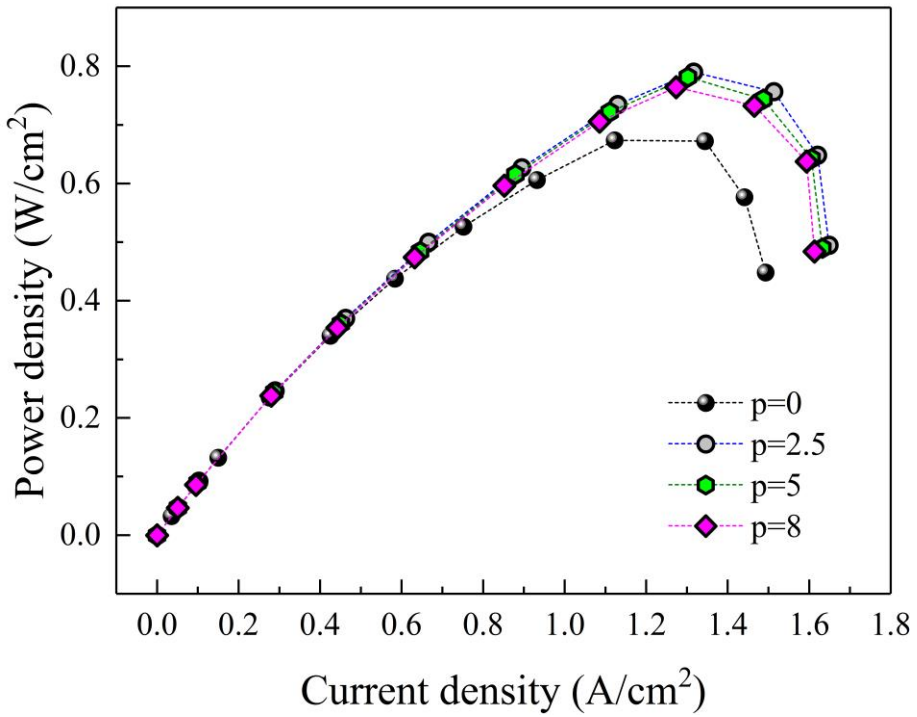

(b)

Fig.15 The output performance of the PEMFC with the different value of spatial interval of blocks. (a) Polarization curves; (b) Power curves.(Case D**)**

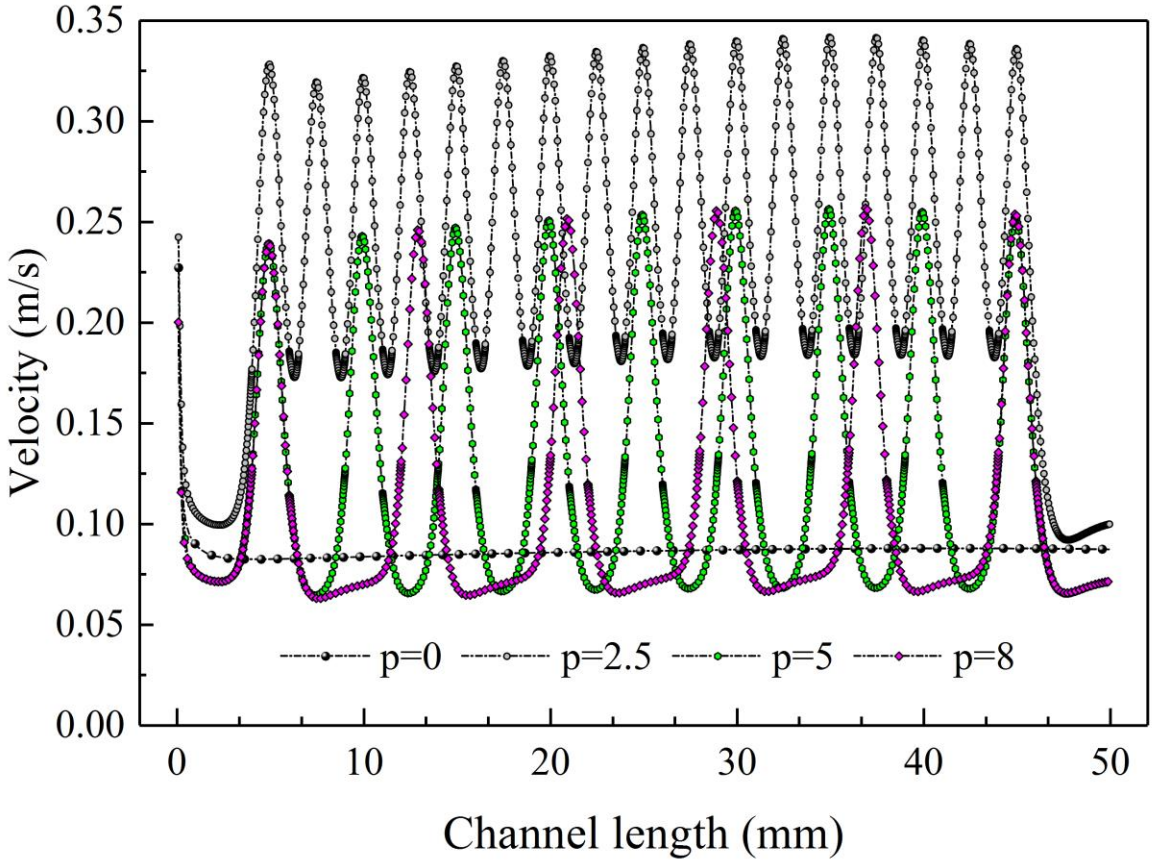

Fig.16 Velocity distribution with the different value of spatial interval of blocks at Line 2 at 0.3V. (*z*=-0.235mm, Case D)**.**

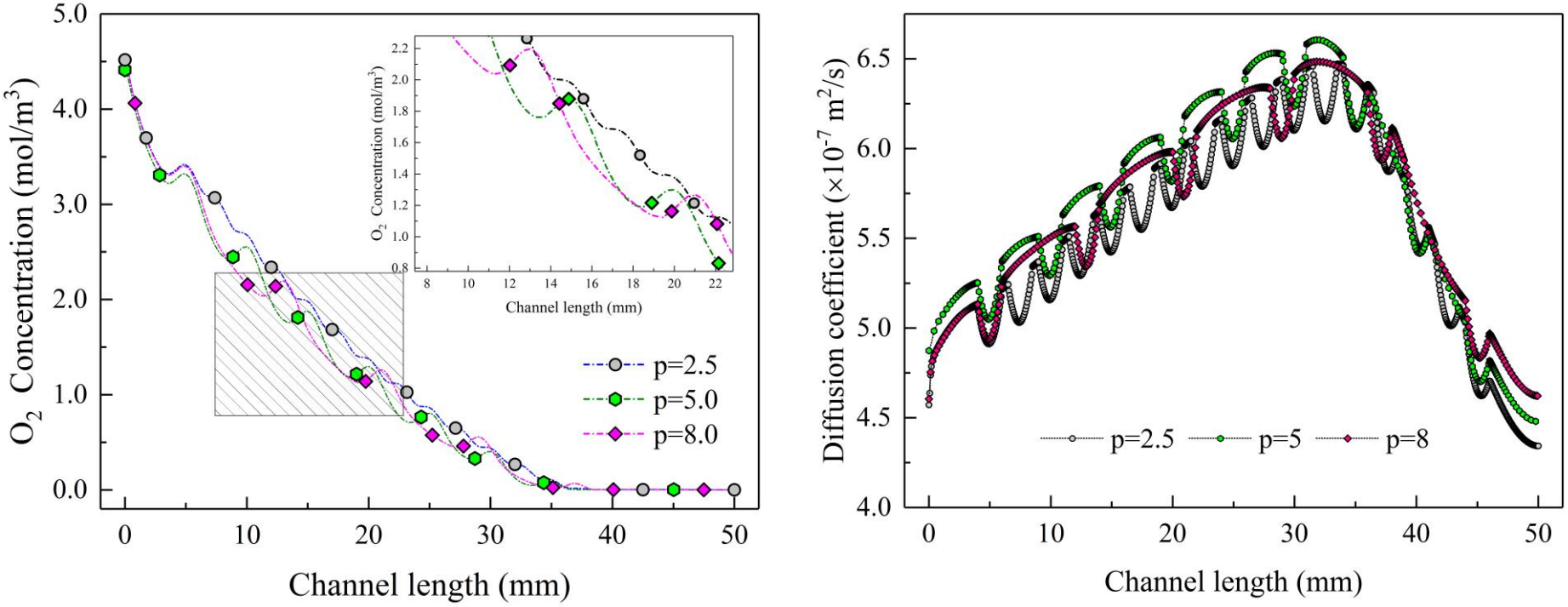

Fig.17 Mass transfer characteristics with spatial interval of blocks (Case D). (a) Oxygen concentration at Line 1 at 0.3V; (b) Diffusion coefficient of liquid water at Line 2 at 0.3V.

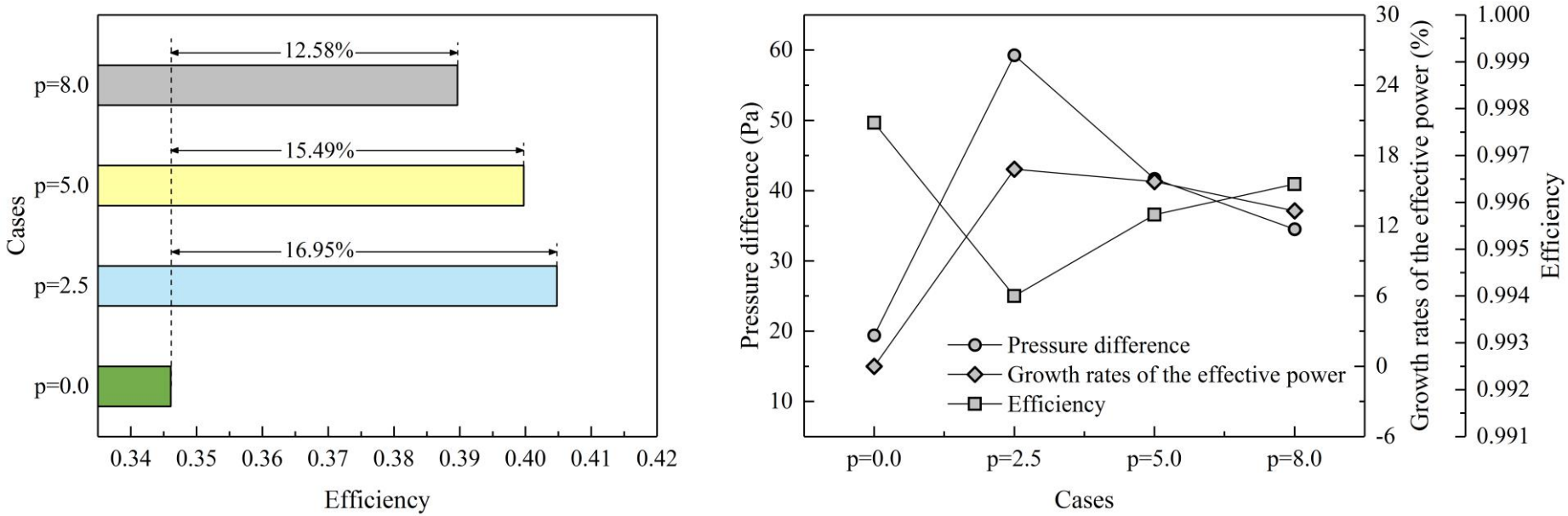

Fig.18 Conversion and loss of electrochemical energy of PEMFC with the different value of spatial interval of blocks (Case D). (a) Comparison of electrochemical efficiency; (b) Comprehensive comparison about loss of energy.